Electronic Band Structures of SbSI in the Para- and Ferroelectric Phases*

Kenji Nako† and M. Balkanski

Laboratoire de Physique des Solides, associé au Centre National de la Recherche Scientifique, Université de Paris VI, 4, Place Jussieu, 75230 Paris Cedex 05 France

(Received 2 April 1973)

The electronic band structures of the ferroelectric semiconductor SbSI, whose crystal structure is very complex compared with the crystals for which the band calculations have been made up to the present, have been calculated by the pseudopotential method in the para- and ferroelectric phases. It is shown that this material has an indirect gap (about 1.4 eV) in both phases and that the smallest direct gap exists at the U point on the surface of the Brillouin zone. It is also found that the optical absorption edge shows the dichroism and electro-optic effect as observed in the experiments. As for the correlation of the band structures with the ferroelectric phase transition (the transition temperature is about 22 °C) it is shown that some bands greatly change their energy values at the phase transition, in particular, the bands at the U point. Further, the dielectric constants have been calculated and compared with the experimental result.

I. INTRODUCTION

Recently, there has been considerable interest in SbSI, which shows a ferroelectric phase transition[1] and semiconducting properties.[2,3] Although phonon-related phenomena[4-9] in SbSI have been extensively investigated, much less is known about its electronic band structure[10-12] and corresponding optical properties.[3,13-16]

One of the purposes of this work is to bring up the essential band-structure features of SbSI and to investigate the correlation between the semiconducting and ferroelectric properties. For this purpose, the band structure of the paraelectric phase and that of the ferroelectric phase have been calculated by the pseudopotential method and compared to each other.

The experimental results are at present insufficient, but the following facts are known for the optical properties.

(i) The absorption edge is about 1.8 eV for the electric field of the incident light parallel to the crystal $\vec{c}$ axis, which is also the polarization axis ($\vec{E} \parallel \vec{c}$), and 1.9 eV for that perpendicular to the $\vec{c}$ axis ($\vec{E} \perp \vec{c}$) in the paraelectric phase.[13]

(ii) In the ferroelectric phase the absorption spectra for $\vec{E} \parallel \vec{c}$ and $\vec{E} \perp \vec{c}$ have line shapes similar to those in the paraelectric phase.[3,13]

(iii) The shift of the absorption edge is about +0.1 eV, going from the paraelectric to the ferroelectric phase.[3,14] This value is the difference of the absorption edges at 5 °C (ferroelectric phase) and at 35 °C (paraelectric phase). Then, strictly speaking, this value includes the effect of the change of the lattice constants, in addition to the proper edge shift between both phases due to the polarization. (The edge at the transition point is 0.02–0.03 eV.) In the band calculations, however, the lattice constants at 5 and 35 °C have been employed; therefore the calculated value should be compared with the difference of the edges at these two temperatures.

(iv) The absorption edge may correspond to direct transitions which are electric dipole allowed.

(v) Below this direct absorption edge there exists also a weak absorption which may be due to indirect transitions.[13,15]

(vi) The observed reflectivities in both phases below 3.5 eV are very similar to each other for various polarizations of the incident light.[16]

(vii) Fine structure has been observed[16] in the reflectivity spectra in the range 2–3.5 eV. In addition, the measured reflectances for $\vec{E} \parallel \vec{c}$ and $\vec{E} \perp \vec{c}$ show a large anisotropy in the electronic properties of SbSI.

(viii) The measured dielectric constant has three peaks in the range 2–6 eV for the case of $\vec{E} \parallel \vec{c}$ in the paraelectric phase.[12]

Of these facts, (i), (ii), and (iv) will be employed to determine the pseudopotentials, and the others will be used as the checks for these pseudopotentials. Although several experiments of photoconductivity[2,3,17] have been made in addition to these, the photoconductivity will not be considered in the following discussion, because this phenomenon is also related to impurities or defects.

In Sec. II and the Appendix, the symmetry properties of SbSI crystal structures are briefly given for both the para- and ferroelectric phases. In particular, the selection rules for the optical transitions are considered for both phases. Since the SbSI crystal structures are very anisotropic, this consideration, connected with facts (ii) and (iv), is very useful to the determination of those critical points in the Brillouin zone at which the optical transition gives rise to the absorption edge.

In Sec. III, it is shown that the matrix element

of the pseudopotential is written as the sum of the products of atomic form factors and atomic structure factors of each atomic species, and that the atomic structure factors of the ferroelectric phase can be related to those of the paraelectric phase in a simple way. The atomic form factors are determined in the first part of Sec. IV. In this section, band calculations in the paraelectric phase have been made, by using the tentative atomic form factors, which were chosen so as to best fit the values obtained up to the present for other crystals. Then these atomic form factors have been slightly changed, and the band structures recalculated. In this way, the final atomic form factors have been determined in order to give the correct values of the absorption edges for $\vec{E} \parallel \vec{c}$ and $\vec{E} \perp \vec{c}$ in the paraelectric phase [fact (i)]. In the rest of Sec. IV, the calculated results of the band structures in both the para- and ferroelectric phases are given together with the calculated dielectric constants in the paraelectric phase.

In Sec. V, the calculated results are compared with the experimental results [facts (iii) and (v)–(viii)]. The agreement is shown to be good if the uncertainty of the calculation and the scarcity of experimental data is taken into account. The correlation of the band structures with the ferroelectric phase transition is also discussed by comparing the band structures of the para- and ferroelectric phases. Furthermore, the general features of the band structures for complex crystals deduced from this work for SbSI are summarized. In Sec. VI the conclusions are given.

II. SYMMETRY PROPERTIES OF SbSI CRYSTAL STRUCTURES

In this section, the symmetry properties of SbSI that are used in the following discussion are briefly summarized; details are given in the Appendix. It should be noted here that the crystal $\vec{c}$ axis, which is also the polarization axis, is taken as parallel to the $\vec{y}$ axis in order to be coincident with the nomenclature of Slater's book,[18] where the symmetry properties of the paraelectric phase of SbSI crystals are considered in detail.

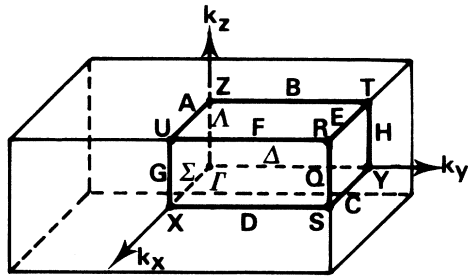

FIG. 2. First Brillouin zone of the SbSI crystal structures. It should be noted that the y direction is taken as parallel to the crystal $\vec{c}$ axis.

The crystal structure of SbSI is given schematically in Fig. 1, where only one double chain of SbSI is shown. This crystal belongs to the orthorhombic system and has actually two double chains in a unit cell (then four SbSI molecules in a unit cell). The arrows in Fig. 1 show the displacements of the Sb and S atoms from the paraelectric to the ferroelectric phase. (The transition temperature is about 22 °C).

The position of jth atom ($j = 1, \ldots, 4$) of the atomic species α(α = Sb, S, or I) in any unit cell is given by

$$\vec{R}_j^{(\alpha)} = \vec{R}_{\text{cell}} + \vec{\tau}_j^{(\alpha)}, \tag{1}$$

where $\vec{R}_{\text{cell}}$ is the translation vector of the orthorhombic system and indicates the considered unit cell. The vector $\vec{\tau}_j^{(\alpha)}$ represents the nonprimitive translation, which is written

$$\vec{\tau}_j^{(\alpha)} = \lambda_j^{(\alpha)} \vec{t}_x + \mu_j^{(\alpha)} \vec{t}_y + \nu_j^{(\alpha)} \vec{t}_z. \tag{2}$$

Here $\vec{t}_i$ ($i = x, y, z$) are the primitive translations whose magnitudes[19] are $|\vec{t}_x| = 8.52$ Å, $|\vec{t}_y| = 4.10$ Å, and $|\vec{t}_z| = 10.13$ Å. These values do not change between 5 and 35 °C. The set of the quantities $\lambda_j^{(\alpha)}$, $\mu_j^{(\alpha)}$, and $\nu_j^{(\alpha)}$ is written in the following form for $j = 1, \ldots, 4$:

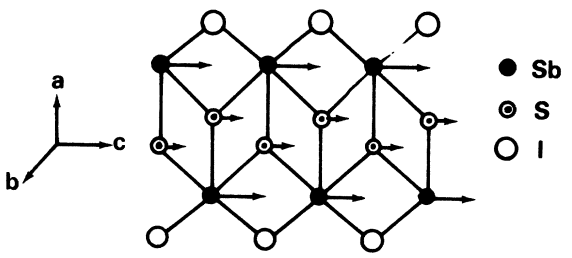

FIG. 1. Crystal structure of SbSI. In this figure only the one double chain is shown. The arrows represents the atomic displacements from the paraelectric phase to the ferroelectric phase.

TABLE I. Atomic positions of each atom in the unit cell of SbSI crystals.

	Para (35 °C)[a]			Ferro (5 °C)[a]		
α	X_α	Y_α	Z_α	X_α	Y_α	Z_α
Sb	0.119	$\frac{1}{4}$	0.124	0.119	0.298	0.124
S	0.840	$\frac{1}{4}$	0.050	0.843	0.261	0.049
I	0.508	$\frac{1}{4}$	0.828	0.508	$\frac{1}{4}$	0.828

[a] The values given here are those measured at 35 °C (paraelectric phase) and at 5 °C (ferroelectric phase) (Ref. 19).

TABLE II. Selection rules of the optical direct transitions at the symmetry points of SbSI in the paraelectric phase.

$\vec{E}\parallel\vec{c}$		$\vec{E}\ \vec{c}$			$\vec{E}\parallel\vec{c}$		$\vec{E}\perp\vec{c}$	
y[a]		x[a]	z[a]		y[a]	x[a]	z[a]	
Γ_1	Γ_4	Γ_6	Γ_8	$\begin{pmatrix}R_1\\R_2\end{pmatrix}$[b]	$\begin{pmatrix}R_1\\R_2\end{pmatrix}$[b]	$\begin{pmatrix}R_1\\R_2\end{pmatrix}$[b]	$\begin{pmatrix}R_2\\R_1\end{pmatrix}$[b]	
Γ_2	Γ_3	Γ_5	Γ_7					
Γ_3	Γ_2	Γ_8	Γ_6					
Γ_4	Γ_1	Γ_7	Γ_5	$\begin{pmatrix}S_1\\S_2\end{pmatrix}$[b]	$\begin{pmatrix}S_2\\S_1\end{pmatrix}$[b]	$\begin{pmatrix}S_1\\S_2\end{pmatrix}$[b]	$\begin{pmatrix}S_2\\S_1\end{pmatrix}$[b]	
Γ_5	Γ_8	Γ_2	Γ_4					
Γ_6	Γ_7	Γ_1	Γ_3					
Γ_7	Γ_6	Γ_4	Γ_2					
Γ_8	Γ_5	Γ_3	Γ_1	T_1	T_2	T_1	T_2	
				T_2	T_1	T_2	T_1	
X_1	X_2	X_1	X_1					
X_2	X_1	X_2	X_2	$\begin{pmatrix}U_1\\U_2\end{pmatrix}$[b]	$\begin{pmatrix}U_4\\U_3\end{pmatrix}$[b]	$\begin{pmatrix}U_7\\U_8\end{pmatrix}$[b]	$\begin{pmatrix}U_8\\U_7\end{pmatrix}$[b]	
Y_1	Y_1	Y_1	Y_2					
Y_2	Y_2	Y_2	Y_1	$\begin{pmatrix}U_3\\U_4\end{pmatrix}$[b]	$\begin{pmatrix}U_2\\U_1\end{pmatrix}$[b]	$\begin{pmatrix}U_5\\U_6\end{pmatrix}$[b]	$\begin{pmatrix}U_6\\U_5\end{pmatrix}$[b]	
Z_1	Z_2	Z_1	Z_1					
Z_2	Z_1	Z_2	Z_2					
				$\begin{pmatrix}U_5\\U_6\end{pmatrix}$[b]	$\begin{pmatrix}U_8\\U_7\end{pmatrix}$[b]	$\begin{pmatrix}U_3\\U_4\end{pmatrix}$[b]	$\begin{pmatrix}U_4\\U_3\end{pmatrix}$[b]	
				$\begin{pmatrix}U_7\\U_8\end{pmatrix}$[b]	$\begin{pmatrix}U_6\\U_5\end{pmatrix}$[b]	$\begin{pmatrix}U_1\\U_2\end{pmatrix}$[b]	$\begin{pmatrix}U_2\\U_1\end{pmatrix}$[b]	

[a] The character y, x, or z means that the electric field of the incident light is parallel to the y, x, or z direction.

[b] The connected states are degenerate due to the time reversal symmetry.

$$(\lambda_j^{(\alpha)}, \mu_j^{(\alpha)}, \nu_j^{(\alpha)}) = (X_\alpha, Y_\alpha, Z_\alpha),$$

$$(-X_\alpha, Y_\alpha+\tfrac{1}{2}, -Z_\alpha), \quad (-X_\alpha+\tfrac{1}{2}, Y_\alpha+\tfrac{1}{2}, Z_\alpha+\tfrac{1}{2}),$$

$$(X_\alpha+\tfrac{1}{2}, Y_\alpha, -Z_\alpha+\tfrac{1}{2}).$$

The values of X_α, Y_α, and Z_α are given in Table I for both phases.[19] Here it should be remarked that $Y^{(\alpha)}=\frac{1}{4}$ for the paraelectric phase. (The displacements in the $\vec{y}$ direction give rise to the spontaneous polarization in the ferroelectric phase.)

The first Brillouin zone is shown in Fig. 2, where the symmetry points and lines are indicated. The space groups of the para- and ferroelectric phases of SbSI crystals[20,21] are D_{2h}^{16} and C_{2v}^{9}, respectively. The symmetry operations of these groups are given in the Appendix, together with the character tables of the irreducible representations of all the groups of $\vec{k}$, but it should be noted here that these two groups are nonsymmorphic and therefore all the states are at least doubly degenerate on the surface of the Brillouin zone. This degeneracy is caused by the spatial-symmetry operations or by the time-reversal operation.

The selection rules of the optical direct transitions are easily obtained from the character tables in the Appendix by using the fact that the $\vec{y}$, $\vec{x}$, and $\vec{z}$ components of the electric field of the incident light transform according to the irreducible representations Γ_4, Γ_6, and Γ_8 in the paraelectric phase and Γ_1, Γ_4, and Γ_2 in the ferroelectric phase, respectively. The results at the symmetry points are given in Tables II and III. Similar results can be obtained for the symmetry lines. These tables should be read as follows: If the states in the columns $\vec{E}\parallel\vec{c}$ and $\vec{E}\perp\vec{c}$ are different (for example, at the points Γ and U), the corresponding direct transitions give rise to an optical dichroism such as that observed at the absorption edges [fact (i) in Sec. I]. Thus, the comparison of Tables II and III gives the important conclusion that the direct transitions at only the points Γ and U (and lines Δ and F) cause the optical dichroism both in the para- and in the ferroelectric phases in the same way. For example, at point X, the dichroism exists in the paraelectric phase but not in the ferroelectric phase. From this fact, and the experimental facts (i), (ii) and (iv) mentioned in Sec. I, it is concluded that the absorption edges of SbSI in both phases correspond to the point Γ or U (or the line Δ or F). The symmetry consideration is hence very useful for the determination of the critical point at which the optical transition gives rise to the absorption edge, for materials with highly anisotropic crystal structures such as SbSI.

In the rest of this section, an intuitive discussion about the band structures of SbSI is given in order to clarify the characters of the electronic structures. For simplicity, this discussion is limited only to the points Γ and U in the paraelectric phase. First, the linear-combination-of-atomic-orbitals (LCAO) model is considered. It is reasonable from

TABLE III. Selection rules of the optical direct transitions at the symmetry points of SbSI in the ferroelectric phase.

$\vec{E}\parallel\vec{c}$		$\vec{E}\perp\vec{c}$			$\vec{E}\parallel\vec{c}$		$\vec{E}\perp\vec{c}$	
y[a]		x[a]	z[a]		y[a]	x[a]	z[a]	
Γ_1	Γ_1	Γ_4	Γ_2	$\begin{pmatrix}R_1\\R_2\end{pmatrix}$[b]	$\begin{pmatrix}R_1\\R_2\end{pmatrix}$[b]	$\begin{pmatrix}R_4\\R_3\end{pmatrix}$[b]	$\begin{pmatrix}R_3\\R_4\end{pmatrix}$[b]	
Γ_2	Γ_2	Γ_3	Γ_1					
Γ_3	Γ_3	Γ_2	Γ_4					
Γ_4	Γ_4	Γ_1	Γ_3	$\begin{pmatrix}R_3\\R_4\end{pmatrix}$[b]	$\begin{pmatrix}R_3\\R_4\end{pmatrix}$[b]	$\begin{pmatrix}R_2\\R_1\end{pmatrix}$[b]	$\begin{pmatrix}R_1\\R_2\end{pmatrix}$[b]	
X_1	X_1	X_1	X_1	S_1	S_1	S_1	S_1	
$\begin{pmatrix}Y_1\\Y_2\\Y_3\\Y_4\end{pmatrix}$[b]	$\begin{pmatrix}Y_1\\Y_2\\Y_3\\Y_4\end{pmatrix}$[b]	$\begin{pmatrix}Y_4\\Y_3\\Y_2\\Y_1\end{pmatrix}$[b]	$\begin{pmatrix}Y_2\\Y_1\\Y_4\\Y_3\end{pmatrix}$[b]	T_1	T_1	T_1	T_1	
				$\begin{pmatrix}U_1\\U_2\end{pmatrix}$[b]	$\begin{pmatrix}U_1\\U_2\end{pmatrix}$[b]	$\begin{pmatrix}U_4\\U_3\end{pmatrix}$[b]	$\begin{pmatrix}U_3\\U_4\end{pmatrix}$[b]	
Z_1	Z_1	Z_1	Z_1	$\begin{pmatrix}U_3\\U_4\end{pmatrix}$[b]	$\begin{pmatrix}U_3\\U_4\end{pmatrix}$[b]	$\begin{pmatrix}U_2\\U_1\end{pmatrix}$[b]	$\begin{pmatrix}U_1\\U_2\end{pmatrix}$[b]	

[a] The character y, x, or z means that the electric field of the incident light is parallel to the y, x, or z direction.

[b] The connected states are degenerate due to the time reversal symmetry.

the structure of the double chain to assume that the SbSI molecule consists of the following formula:

the ionic model

$$Sb^{3+}(5s^2)S^{2-}(3s^2,\ 3p_x^2,\ 3p_y^2,\ 3p_z^2)$$

$$I^-(5s^2,\ 5p_x^2,\ 5p_y^2,\ 5p_z^2)$$

or

the covalent model

$$Sb^+(5s^2,\ 5p_y^2)S^-(3s^2,\ 3p_x^2,\ 3p_z^2)I^-(5s^2,\ 5p_x^2,\ 5p_y^2,\ 5p_z^2).$$

In both models, there are 72 valence electrons for four SbSI molecules in a unit cell and thus 36 valence bands. With the use of the LCAO bases constructed from the atomic s and p functions, which are given in Table IV, these 36 valence bands are classified in the following way:

at Γ point,

$$7\Gamma_1+2\Gamma_2+7\Gamma_3+2\Gamma_4+2\Gamma_5+7\Gamma_6+2\Gamma_7+7\Gamma_8$$

and

at U point,

$$7U_1+7U_2+2U_3+2U_4+2U_5+2U_6+7U_7+7U_8\ ,$$

where, in the state Γ_1, Γ_3, Γ_6, Γ_8, U_1, U_2, U_7, or U_8, there are three s-like, two p_x-like, and two p_z-like states, and the state Γ_2, Γ_4, Γ_5, Γ_7, U_3, U_4, U_5, or U_6 consists of two p_y-like states. As for the low-lying conduction bands, these are mainly made of the $5p_x$, $5p_y$, and $5p_z$ functions of Sb in the ionic model or made of the $5p_x$ and $5p_z$ functions of Sb and of the $3p_y$ function of S in the covalent model. The actual crystal of SbSI is, of course, between these two limiting models, but, as seen in the following sections, the ionic model seems preferable.

Next, in the contrary to the LCAO model, the free-electron model is discussed. The free-electron energies at the points Γ and U are listed in Tables V and VI, where the set of h_x, h_y, and h_z designates the reciprocal-lattice vector such that

$$\vec{K}=h_x\vec{b}_x+h_y\vec{b}_y+h_z\vec{b}_z\,, \tag{3}$$

where $\vec{b}_x$, $\vec{b}_y$, and $\vec{b}_z$ are the primitive translation vectors in the reciprocal lattice and

$$\vec{b}_i=(2\pi/|\vec{t}_i\,|^2)\vec{t}_i\quad(i=x,y,z)\,. \tag{4}$$

In these tables, the low-lying 36 states are distinguished from the other states so that the classification of 36 valence bands coincides with that obtained from the LCAO point of view. It is reasonably expected from these tables that the top of the valence band is Γ_2, Γ_3, Γ_4, Γ_6, or Γ_7, and the bottom of the conduction band is Γ_1, Γ_5, or Γ_8 at the Γ point, while at the U point the bottom of the conduction band is U_1 (U_2) or U_7 (U_8).

As will be seen in Sec. IV, the conjecture men-

TABLE IV. LCAO bases of SbSI at the points Γ and U in the paraelectric phase. In this table the following abbreviations are employed:

$$\Psi_{Sj}^{(\alpha)}=\sum_{R_{\rm cell}} e^{i\vec{k}\cdot\vec{R}_{\rm cell}}\Phi_S^{(\alpha)}(\vec{r}-\vec{R}_{\rm cell}-\vec{\tau}_j^{(\alpha)}),$$

$$\Psi_{p_ij}^{(\alpha)}=\sum_{R_{\rm cell}} e^{i\vec{k}\cdot\vec{R}_{\rm cell}}\Phi_{p_i}^{(\alpha)}(\vec{r}-\vec{R}_{\rm cell}-\vec{\tau}_j^{(\alpha)}),$$

where $\Phi_S^{(\alpha)}$ and $\Psi_{p_i}^{(\alpha)}$ ($p_i=p_x,\ p_y,\ p_z$) are the atomic S and p_i functions of the atomic species α ($\alpha=$ Sb, S, I) located at the position $\vec{R}_{\rm cell}+\vec{\tau}_j^{(\alpha)}$ ($j=1,\ \ldots,\ 4$).

Γ_1	$(\Psi_{S1}^{(\alpha)}+\Psi_{S2}^{(\alpha)}+\Psi_{S3}^{(\alpha)}+\Psi_{S4}^{(\alpha)})$,	$(\Psi_{p_x1}^{(\alpha)}-\Psi_{p_x2}^{(\alpha)}-\Psi_{p_x3}^{(\alpha)}-\Psi_{p_x4}^{(\alpha)})$,	$(\Psi_{p_z1}^{(\alpha)}-\Psi_{p_z2}^{(\alpha)}-\Psi_{p_z3}^{(\alpha)}-\Psi_{p_z4}^{(\alpha)})$
Γ_2		$(\Psi_{p_y1}^{(\alpha)}+\Psi_{p_y2}^{(\alpha)}-\Psi_{p_y3}^{(\alpha)}-\Psi_{p_y4}^{(\alpha)})$	
Γ_3	$(\Psi_{S1}^{(\alpha)}+\Psi_{S2}^{(\alpha)}-\Psi_{S3}^{(\alpha)}-\Psi_{S4}^{(\alpha)})$	$(\Psi_{p_x1}^{(\alpha)}-\Psi_{p_x2}^{(\alpha)}+\Psi_{p_x3}^{(\alpha)}-\Psi_{p_x4}^{(\alpha)})$,	$(\Psi_{p_z1}^{(\alpha)}-\Psi_{p_z2}^{(\alpha)}-\Psi_{p_z3}^{(\alpha)}+\Psi_{p_z4}^{(\alpha)})$
Γ_4		$(\Psi_{p_y1}^{(\alpha)}+\Psi_{p_y2}^{(\alpha)}+\Psi_{p_y3}^{(\alpha)}+\Psi_{p_y4}^{(\alpha)})$	
Γ_5		$(\Psi_{p_y1}^{(\alpha)}-\Psi_{p_y2}^{(\alpha)}+\Psi_{p_y3}^{(\alpha)}-\Psi_{p_y4}^{(\alpha)})$	
Γ_6	$(\Psi_{S1}^{(\alpha)}-\Psi_{S2}^{(\alpha)}-\Psi_{S3}^{(\alpha)}+\Psi_{S4}^{(\alpha)})$,	$(\Psi_{p_x1}^{(\alpha)}+\Psi_{p_x2}^{(\alpha)}+\Psi_{p_x3}^{(\alpha)}+\Psi_{p_x4}^{(\alpha)})$,	$(\Psi_{p_z1}^{(\alpha)}+\Psi_{p_z2}^{(\alpha)}-\Psi_{p_z3}^{(\alpha)}-\Psi_{p_z4}^{(\alpha)})$
Γ_7		$(\Psi_{p_y1}^{(\alpha)}-\Psi_{p_y2}^{(\alpha)}-\Psi_{p_y3}^{(\alpha)}+\Psi_{p_y4}^{(\alpha)})$	
Γ_8	$(\Psi_{S1}^{(\alpha)}-\Psi_{S2}^{(\alpha)}+\Psi_{S3}^{(\alpha)}-\Psi_{S4}^{(\alpha)})$,	$(\Psi_{p_x1}^{(\alpha)}+\Psi_{p_x2}^{(\alpha)}-\Psi_{p_x3}^{(\alpha)}-\Psi_{p_x4}^{(\alpha)})$,	$(\Psi_{p_z1}^{(\alpha)}+\Psi_{p_z2}^{(\alpha)}+\Psi_{p_z3}^{(\alpha)}+\Psi_{p_z4}^{(\alpha)})$
U_1[a]	$(\Psi_{S1}^{(\alpha)}+\Psi_{S2}^{(\alpha)}-i\Psi_{S3}^{(\alpha)}-i\Psi_{S4}^{(\alpha)})$,	$(\Psi_{p_x1}^{(\alpha)}-\Psi_{p_x2}^{(\alpha)}+i\Psi_{p_x3}^{(\alpha)}-i\Psi_{p_x4}^{(\alpha)})$,	$(\Psi_{p_z1}^{(\alpha)}-\Psi_{p_z2}^{(\alpha)}-i\Psi_{p_z3}^{(\alpha)}+i\Psi_{p_z4}^{(\alpha)})$
U_3[a]		$(\Psi_{p_y1}^{(\alpha)}+\Psi_{p_y2}^{(\alpha)}+i\Psi_{p_y3}^{(\alpha)}+i\Psi_{p_y4}^{(\alpha)})$	
U_5[a]		$(\Psi_{p_y1}^{(\alpha)}-\Psi_{p_y2}^{(\alpha)}-i\Psi_{p_y3}^{(\alpha)}+i\Psi_{p_y4}^{(\alpha)})$	
U_7[a]	$(\Psi_{S1}^{(\alpha)}-\Psi_{S2}^{(\alpha)}+i\Psi_{S3}^{(\alpha)}-i\Psi_{S4}^{(\alpha)})$,	$(\Psi_{p_x1}^{(\alpha)}+\Psi_{p_x2}^{(\alpha)}-i\Psi_{p_x3}^{(\alpha)}-i\Psi_{p_x4}^{(\alpha)})$,	$(\Psi_{p_z1}^{(\alpha)}+\Psi_{p_z2}^{(\alpha)}+i\Psi_{p_z3}^{(\alpha)}+i\Psi_{p_z4}^{(\alpha)})$

[a] The states with the irreducible representations U_2, U_4, U_6, and U_8 are degenerate with those with U_1, U_3, U_5, and U_9, respectively.

TABLE V. Free-electron energies at the Γ point of SbSI crystal in the paraelectric phase. The energy is written $E = 1.504\ G$ (eV), $G = 1.37\ h_x^2 + 5.90\ h_y^2 + 0.974\ h_z^2$.

h_x	h_y	h_z	G	States							No.
0	0	0	0.0	Γ_1							1
0	0	±1	0.97			Γ_3			Γ_6		2
±1	0	0	1.37			Γ_3				Γ_8	2
±1	0	±1	2.34	Γ_1		Γ_3			Γ_6	Γ_8	4
0	0	±2	3.90	Γ_1						Γ_8	2
±1	0	±2	5.27	Γ_1		Γ_3			Γ_6	Γ_8	4
±2	0	0	5.48	Γ_1					Γ_6		2
0	±1	0	5.90						Γ_6	Γ_7	2
±2	0	±1	6.45	Γ_1		Γ_3			Γ_6	Γ_8	4
0	±1	±1	6.87	Γ_1			Γ_4	Γ_5		Γ_8	4
±1	±1	0	7.27		Γ_2	Γ_3		Γ_5		Γ_8	4
±1	±1	±1[a]	8.24		Γ_2	Γ_3	Γ_4		Γ_6	Γ_7	5
±1	±1	±1[a]	8.24	Γ_1				Γ_5		Γ_8	3
0	0	±3	8.73			Γ_3			Γ_6		2
±2	0	±2	4.38	Γ_1		Γ_3			Γ_6	Γ_8	4
0	±1	±2	9.80		Γ_2	Γ_3			Γ_6	Γ_7	4

[a]It should be noted that the case (±1, ±1, ±1) is divided into two parts (see the text).

tioned here is the case; that is, the classification of 36 valence bands is correct, and the top of the valence band is Γ_6 and $U_5(U_6)$, while the bottom of the conduction band is Γ_8 and $U_7(U_8)$. Thus the band structures of SbSI are, on the one hand, LCAO like, and, on the other hand, free-electron like.

III. PSEUDOPOTENTIAL METHOD

The band-calculation method employed in this work is the pseudopotential method.[22] Although the precise determination of the pseudopotentials needs many good experimental results and at present the experiments are insufficient for this purpose, this method has been chosen for its relatively easy use for the calculation of the band structure for materials with very complicated crystal structures such as SbSI, if the pseudopotentials are once obtained. Since there is little knowledge of the electronic structures of SbSI, for the moment the pseudopotentials obtained for various other crystals will be used for the determination of the pseudopotentials which are necessary for the band calculations of SbSI, instead of the usual process in which the pseudopotentials are determined from the comparison with the experiments. The details of this will be described in Sec. IV; this section is devoted to the discussion of the parameters which are connected with the crystal structures and of the related quantities.

As usual, the crystal pseudopotential is taken as the sum of the atomic pseudopotentials as follows:

$$V(\vec{r}) = \sum_{\alpha} \sum_{\vec{R}_{\text{cell}}} \sum_{j} v_{\alpha}(\vec{r} - \vec{R}_{\text{cell}} - \vec{\tau}_j^{(\alpha)}), \tag{5}$$

where $v_\alpha(\vec{r})$ is the atomic pseudopotential of the atomic species α and is assumed to be local and energy independent. The Fourier transform of this pseudopotential (which is also its matrix element between plane waves) is written

$$V(\vec{K}) = \sum_{\alpha} S_{\alpha}(\vec{K}) \frac{\Omega_\alpha}{\Omega_c} v_{\alpha}(\vec{K}), \tag{6}$$

where Ω_α and Ω_c are the normalization volume given for the atomic species α and the volume of a unit cell, respectively. In Eq. (6) the quantities $S_\alpha(\vec{K})$ and $v_\alpha(\vec{K})$ are the atomic structure factor and the atomic form factor, respectively, for the atomic species α, and are defined by

$$S_{\alpha}(\vec{K}) = \sum_{j} e^{i\vec{K}\cdot\vec{\tau}_j^{(\alpha)}}, \tag{7}$$

$$v_{\alpha}(\vec{K}) = \frac{1}{\Omega_\alpha} \int v_{\alpha}(\vec{r}) e^{i\vec{K}\cdot\vec{r}}\, d^3\vec{r}, \tag{8}$$

where the integral is taken over the volume Ω_α.

The atomic structure factors can be easily calculated, because the atomic positions in the unit cell are known. Since the SbSI crystal in the paraelectric phase has an inversion center, the atomic structure factors are real and are written as follows, with the use of the quantities given in Table I and Eq. (3):

$$S_{\alpha}^{(p)}(\vec{K}) = 4\cos 2\pi[(X_\alpha^{(p)} + \tfrac{1}{4})h_x + \tfrac{1}{4}h_y + \tfrac{1}{4}h_z] \times \cos 2\pi[-\tfrac{1}{4}h_x + (Z_\alpha^{(p)} - \tfrac{1}{4})h_z], \tag{9}$$

where the index p is introduced for indicating that the quantities are for the paraelectric phase. For the ferroelectric phase, the atomic structure factors are not real. For example,

TABLE VI. Free-electron energies at the U point of the SbSI crystal in the paraelectric phase. The energy is written $E = 1.504\,G$ (eV), $G = 1.37\,(h_x+\frac{1}{2})^2 + 5.90\,h_y^2 + 0.974\,(h_z+\frac{1}{2})^2$.

h_y	h_z	G	States								No.
0	0										
0	−1	0.62	U_1	U_2					U_7	U_8	4
0	0										
−1	−1										
0	0										
0	−2	2.70	U_1	U_2					U_7	U_8	4
0	1										
−1	−2										
0	0										
1	−1	3.50	U_1	U_2					U_7	U_8	4
0	0										
−2	−1										
0	1										
1	−2	5.58	U_1	U_2					U_7	U_8	4
0	1										
−2	−2										
0	0										
±1	−1	6.52	U_1	U_2	U_3	U_4	U_5	U_6	U_7	U_8	8
0	0										
−1	−1										
0	2										
0	−3	6.86	U_1	U_2					U_7	U_8	4
−1	2										
0	−3										
0	1										
±1	−2	8.60	U_1	U_2	U_3	U_4	U_5	U_6	U_7	U_8	8
0	1										
±1	−2										
2	0										
0	−1	9.26	U_1	U_2					U_7	U_8	4
0	0										
−3	−1										
1	0										
±1	−1	9.40	U_1	U_2	U_3	U_4	U_5	U_6	U_7	U_8	8
1	0										
±1	−2										
−2	0										
±1	−1										

$$S_\alpha^{(f)}(\vec{K}) = 4e^{2\pi i[\Gamma_\alpha^{(f)} - 1/4]h_y} \times \cos 2\pi[(X_\alpha^{(f)} + \tfrac{1}{4})h_x + \tfrac{1}{4}h_y + \tfrac{1}{4}h_z] \times \cos 2\pi[-\tfrac{1}{4}h_x + (Z_\alpha^{(f)} - \tfrac{1}{4})h_z]. \quad (10)$$

Since $X_\alpha^{(f)}$ and $Z_\alpha^{(f)}$ are almost the same as $X_\alpha^{(p)}$ and $Z_\alpha^{(p)}$ (as is seen in Table I), $S_\alpha^{(f)}(\vec{K})$ is approximated as

$$S_\alpha^{(f)}(\vec{K}) \simeq e^{2\pi i[\Gamma_\alpha^{(f)} - (1/4)]h_y} S_\alpha^{(p)}(\vec{K}). \quad (11)$$

The factors in the exponent represent the displacements of atoms in the ferroelectric phase relative to the atomic positions in the paraelectric phase and their magnitudes at 5 °C are given in Table VII. It is seen in this table that the displacement of the Sb atom is about 5% of the length of the unit cell.

Since the displacement of S and I atoms are small compared with that of the Sb atom, the difference of the pseudopotentials between the ferro- and paraelectric phases is approximated as follows, using Eq. (11):

TABLE VII. Factor representing the displacements of each atom of SbSI in the ferroelectric phase at 5 °C.

α	$Y_\alpha^{(f)} - \frac{1}{4}$	$(Y_\alpha^{(f)} - \frac{1}{4})\lvert\vec{t}_y\rvert$ [a]
Sb	0.048	0.372 a.u.
S	0.011	0.085 a.u.
I	0.0	0.0

[a] $\lvert\vec{t}_y\rvert = 7.75$ a.u.; 1 a.u. $= 5.29 \times 10^{-9}$ cm.

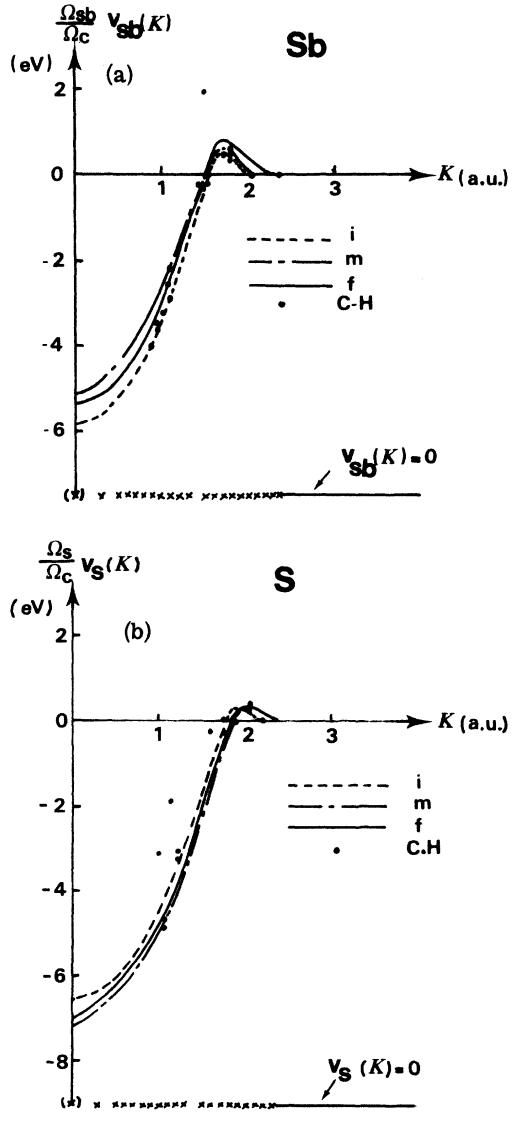

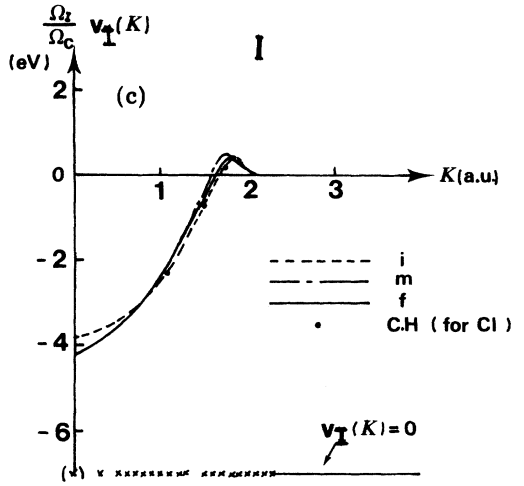

FIG. 3. Atomic form factors of (a) Sb, (b) S, and (c) I. It should be noted that these are corrected by the volume factor Ω_α/Ω_c. The symbols i, m, and f represent three different atomic form factors of each atom with which the band structures have been examined, and the final atomic form factors are those of f (see the text). The dots in these figures are the values of the atomic form factors obtained for other crystals [M. L. Cohen and V. Heine, Solid State Phys. 24, 37 (1970)]. The cross points at the bottom show the values of κ that are necessary in the band calculations of SbSI.

$$\Delta V(\vec{K}) \equiv V^{(f)}(\vec{K}) - V^{(p)}(\vec{K}) \simeq -[1-\cos\Delta Y_{Sb}K_y + i\sin\Delta Y_{Sb}K_y]S_{Sb}^{(p)}(\vec{K})(\Omega_{Sb}/\Omega_c)v_{Sb}(\vec{K}), \quad (12)$$

where $\Delta Y_{Sb}=(Y_{Sb}^{(f)}-\frac{1}{4})\,|\,\vec{t}_y\,|$ is the displacement of the Sb atom. For large $|\vec{K}|$, the atomic form factor $v_{Sb}(\vec{K})$ becomes very small, and then Eq. (12) is farther approximated as

$$\Delta V(\vec{K}) \simeq -\left[\frac{1}{2}\left(\frac{P_s}{Ne^*}\right)^2 K_y^2 + i\left(\frac{P_s}{Ne^*}\right)K_y\right] \times S_{Sb}^{(p)}(\vec{K})\frac{\Omega_{Sb}}{\Omega_c}v_{Sb}(\vec{K}), \quad (13)$$

where $P_s \simeq Ne^*\Delta Y_{Sb}$ is the spontaneous polarization in the ferroelectric phase, and N and e^* are the number of Sb atoms in the unit volume and the effective charge, respectively. Equation (13) means that the spontaneous polarization and the atomic form factor of the Sb atom contribute mainly to the difference of the pseudopotentials and then to the difference of the band structures between both phases.

In connection with this difference of the pseudopotentials, it is useful to introduce the concept of the polarization potential,[23] which is analogous to that of the deformation potential. The polarization potential is defined as the change of the band energy due to the unit polarization; that is, the energy change of the nth band at the point $\vec{k}$, $\Delta E_n(\vec{k})$, is written

$$\Delta E_n(\vec{k}) = \sum_{i,j} b_{ij}^{(n)}(\vec{k})P_iP_j, \quad (14)$$

where P_i is the ith component of the polarization and $b_{ij}^{(n)}(\vec{K})$ is the corresponding polarization potential tensor. This quantity is defined in the same way for the pair band. These polarization potentials can be determined from the band calculations by comparing the band energies of the para- and ferroelectric phases, as discussed in later sections. Here the electro-optic effect on the absorption edge is considered in terms of the polarization potential. When the external electric field is applied in the direction of the spontaneous polarization, the energy change of the absorption edge is expressed as

$$\Delta E_G = bP^2, \quad (15)$$

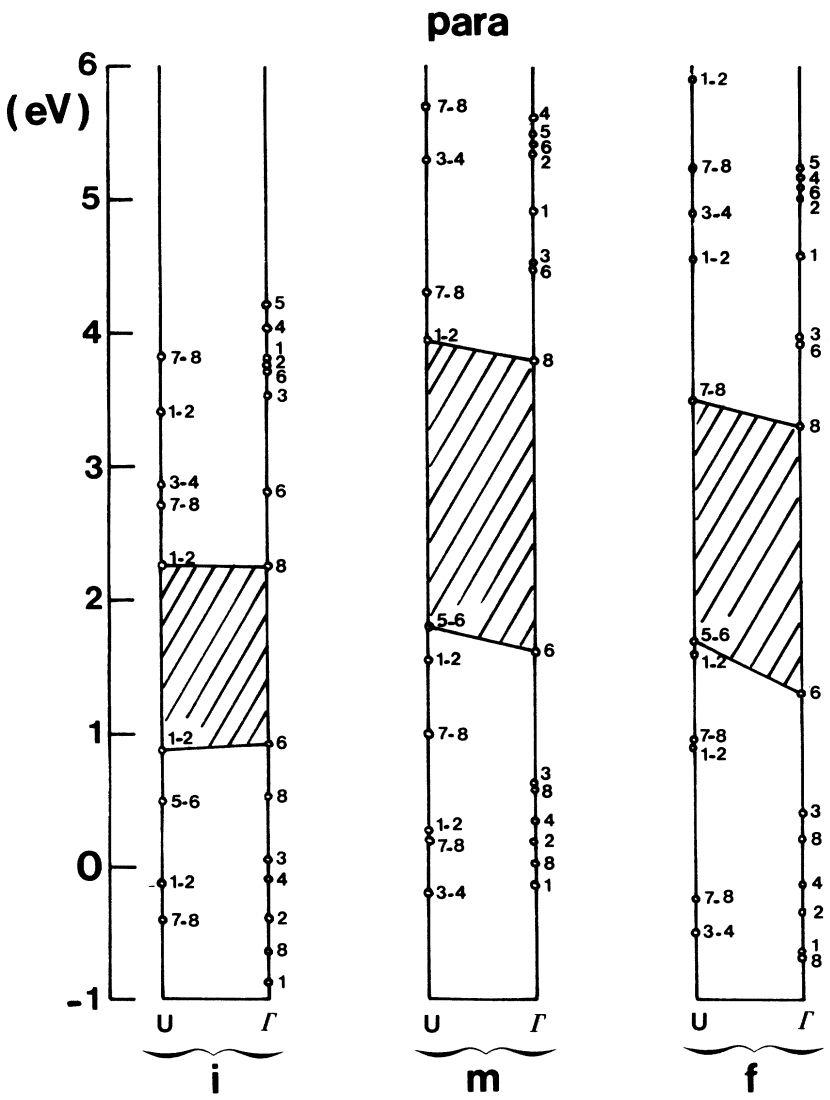

FIG. 4. Changes of the band energies for three different sets of the atomic form factors at the points Γ and U of SbSI in the paraelectric phase.

where P is the sum of the spontaneous and induced polarizations such as

$$\vec{P} = \vec{P}_s(T) + \chi \vec{E}_{\text{ext}}, \tag{16}$$

where $\vec{P}_s(T)$ is the spontaneous polarization and χ is the electric susceptibility. Then the linear and quadratic electro-optic effects are expected for the ferro- and paraelectric phases, respectively, in the following way:

$$\Delta E_G^{(f)} = 2b\chi^{(f)} \vec{P}_s(T) \vec{E}_{\text{ext}}, \tag{17}$$

$$\Delta E_G^{(p)} = b\chi^{(p)2} E_{\text{ext}}^2. \tag{18}$$

These electro-optic effects have been measured for the absorption edges of SbSI in both phases.[13]

IV. BAND STRUCTURES AND OPTICAL PROPERTIES OF SbSI

In this section the calculated results of the band structures and of the dielectric constants of SbSI are given. The determination of the atomic form factors are assumed, as usual, to be local and spherically symmetric, such that $v_\alpha(\vec{K}) = v_\alpha(\kappa)$, where κ is the absolute value of the vector $\vec{K}$. As mentioned in the preceding section, the usual process of the determination of all the atomic form factors from comparison with experiments is impossible, for at present there is little knowledge about the band structures and the optical properties of SbSI, and the experiments are insufficient. Therefore, the energy levels have been calculated only at the points Γ and U of SbSI *in the paraelectric phase* using the tentative atomic form factors, because direct absorption edges have been observed with a relative precision and they correspond to direct transitions at the point Γ or U, as shown in Sec. II. The calculations have then been repeated with the use of the other atomic form factors which have been changed slightly from the

first tentative ones, until the calculated values of the absorption edges for $\vec{E} \parallel \vec{c}$ and $\vec{E} \perp \vec{c}$ coincided with the observed values in the paraelectric phase. Finally the over-all band structures have been calculated using the atomic form factors determined in this way. It should be remarked here that these final atomic form factors contain much uncertainty, because only two experimental results have been used in the above process of the determination of the atomic form factors. This uncertainty can be checked by the comparison of the calculated band structures with the other experimental results and, as will be seen in the Sec. IV, the calculated band structures explain the experiments considerably well.

The first tentative atomic form factors have been determined from those obtained at present for various other crystals. (For the Sb atom, for example, the atomic form factor is determined for the crystals of Sb, AlSb, GaSb, and InSb). In doing so, the following interpolation formula used by Falicov and Lin[24] has been assumed for all the values of κ less than $6^{1/2}$ a.u.:

$$(\Omega_\alpha/\Omega_c)v_\alpha(\kappa)=A_\alpha(\kappa^2-B_\alpha)/(1+e^{C_\alpha(\kappa^2-D_\alpha)}), \quad (19)$$

because the number of κ necessary for the band calculations of SbSI is extremely large, as shown in the bottom of Fig. 3. It should be noted that Eq. (19) contains the volume factor Ω_α/Ω_c. For the values of κ larger than $6^{1/2}$ a.u., it has been also assumed that $v_\alpha(\kappa)=0$. The potential parameters A_α, B_α, C_α, and D_α in Eq. (19) have been chosen so as to best-fit the values of the atomic form factors obtained up to now. These values have been cited by Cohen and Heine[22] for Sb and S atoms and are shown by the dots in Fig. 3. For the atom I there exists no atomic form factor; therefore, that of the atom Cl[22,23] has been used, because the atomic pseudopotential $v_\alpha(\vec{r})$ is mainly due to the nucleus and the core electrons of an α atom and, therefore, it is expected that the atomic pseudopotentials for the atoms with the same valency (for I and Cl, $Z=7$) are approximately the same. This approximation is written

$$\Omega_I v_I(\kappa)\equiv \int v_I(\vec{r})e^{i\kappa r}d^3r \simeq \int v_{Cl}(\vec{r})e^{i\kappa r}d^3r \equiv \Omega_{Cl}v_{Cl}(\kappa). \quad (20)$$

These tentative form factors are shown by the lines i in Fig. 3.

The calculated energy levels at the points Γ and U using these atomic form factors are given by the part i in Fig. 4, where the abbreviated notions are used for the irreducible representations. (For example, the number 8 at the Γ point means that this level belongs to Γ_8 and the double manner 1-2 at the U point represents the degeneracy of the states U_1 and U_2.) Since this result did not give the correct values of the absorption edges in the paraelectric phase [fact (i) in Sec. I], the calculations have been repeated for the other atomic form factors which have been changed slightly from i. One example of the atomic form factors and the calculated results are shown by m in Figs. 3 and 4. The lines f in Fig. 3 represent the final atomic form factors and the corresponding potential parameters are summarized in Table VIII. These give the correct values of the absorption edges in the paraelectric phase; that is, 1.82 eV for $\vec{E} \parallel \vec{c}$ and 1.91 eV for $\vec{E} \perp \vec{c}$. The former edge corresponds to the transition $U_{5-6}^{(v)} - U_{7-8}^{(c)}$ and the latter to the transition $U_{1-2}^{(v)} - U_{7-8}^{(c)}$, where the indices v and c indicate the valence and conduction bands. It should be remarked that the band-edge states at the Γ point are always $\Gamma_6^{(v)}$ and $\Gamma_8^{(c)}$ and that the optical transition between these states is forbidden. It should be also noted that the experimental results used for the determination of the atomic form factors are only the absorption edges *in the paraelectric phase* and not in the ferroelectric phase.

The over-all band structures have been calculated using the atomic form factors f for the symmetry points and lines. The results show that the classification of 36 valence bands is the same as that obtained from the LCAO point of view in Sec. II. The calculated band structures around the forbidden gap in the para- and ferroelectric phases are given in Figs. 5 and 6, respectively, where the same abbreviation of the irreducible representations is employed as in Fig. 4. The same atomic form factors have been used for both phases. The atomic positions which enter into the atomic structure factors, Eqs. (9) and (10), have been those measured at 35 and at 5 °C for the para- and ferroelectric phases.[19] Although these temperatures are indicated in the figures, the effects of the lattice vibrations on the band structures have not been considered in the calculations. It is seen from these figures that the SbSI crystals have an indirect gap in both phases. In the paraelectric phase, the top of the valence band and the bottom of the conduction bands are $U_{5-6}^{(v)}$ and $Z_1^{(c)}$, respectively, and the magnitude of the indirect gap is 1.41 eV. The corresponding value in the ferroelectric phase

TABLE VIII. Parameters of the atomic form factors.

α	A_α [a]	B_α [b]	C_α [b]	D_α [b]
Sb	0.20	2.3	2.8	3.1
S	0.16	3.4	3.4	3.2
I	0.28	2.6	3.6	3.2

[a] The unit of A_α is eV.

[b] The units of B_α, C_α, and D_α are a.u.

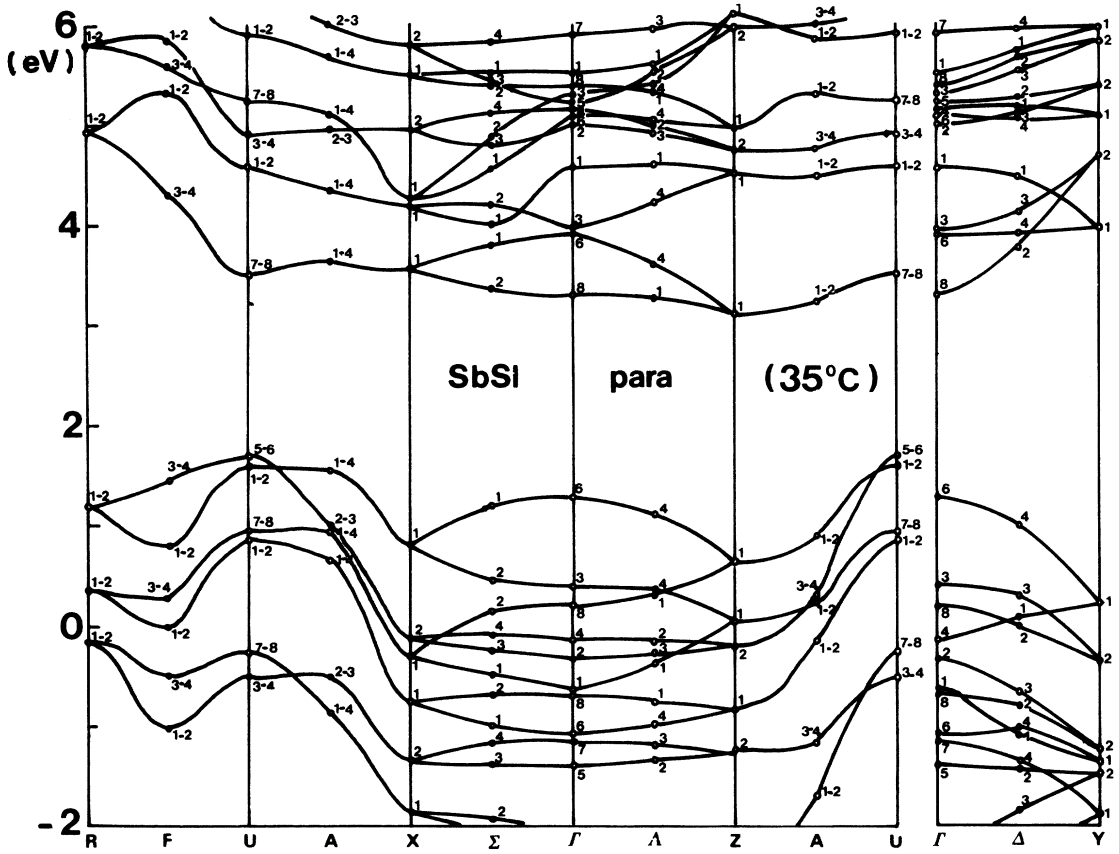

FIG. 5. Band structure of SbSI around the forbidden gap in the paraelectric phase. (The atomic positions at 35 °C are used in the calculation.) The numbers represent the corresponding irreducible representations at the symmetry points and lines.

is 1.43 eV, which is the energy difference of $Z_1^{(c)}$ and $R_{3-4}^{(v)}$. The minima of the direct gap exist at the U point in both phases, thus the direct absorption edges correspond to the optical transitions at the U point in the ferroelectric phase as well as in the paraelectric one. The calculated values of the absorption edges are 1.82 eV for $\vec{E} \parallel \vec{c}$ $(U_{5-6}^{(v)} \rightarrow U_{7-8}^{(c)})$ and 1.91 eV for $\vec{E} \perp \vec{c}$ $(U_{1-2}^{(v)} \rightarrow U_{7-8}^{(c)})$ for the paraelectric phase, and 2.03 eV for $\vec{E} \parallel \vec{c}$ $(U_{3-4}^{(v)} \rightarrow U_{3-4}^{(c)})$ and 1.97 eV for $\vec{E} \perp \vec{c}$ $(U_{1-2}^{(v)} \rightarrow U_{3-4}^{(c)})$ for the ferroelectric one. Thus, the shift of the absorption edges from the para- to the ferroelectric phases is about 0.1~0.2 eV, but the dichroism of the absorption edges is contrary in both phases [facts (ii) and (iii) in Sec. I].

As seen from the figures, the over-all band structures in both phases are generally similar to each other, except for the small shift of the position of energy levels. The remarkable fact to be noted is the splitting of the states at the R point in the ferroelectric phase (these states are degenerate due to the time-reversal symmetry in the paraelectric phase). The features of the over-all band structures of SbSI are the existence of many close-energy levels, the small band width of about 1 eV (thus the large effective mass) and the large anisotropy of the band structures. The third feature is the reflection[25] of the highly anisotropic crystal structures of SbSI; that is, in the direction of the crystal $\vec{c}$ axis the electrons can easily move and thus the band variation with $\vec{k}$ is relatively large along the lines Δ and F, which are parallel to the $\vec{y}$ direction (or the crystal $\vec{c}$ axis). The first and second features are related to the fact that there are many atoms in a unit cell of SbSI and the dimension of the unit cell is considerably large. Furthermore, the low symmetry of the crystal structures contributes to the second feature, because in this case there are many states with the same symmetry and they cancel one another.

In Fig. 7, an example of the convergence of the energies of the states Γ_1 and Γ_2 is given for the paraelectric phase. The convergence of the other states is almost the same. The quantity G represents the number of plane waves employed in the band calculations and is connected with the kinetic energy of the plane-wave state with the wave vector $(\vec{K}+\vec{k})$ such that

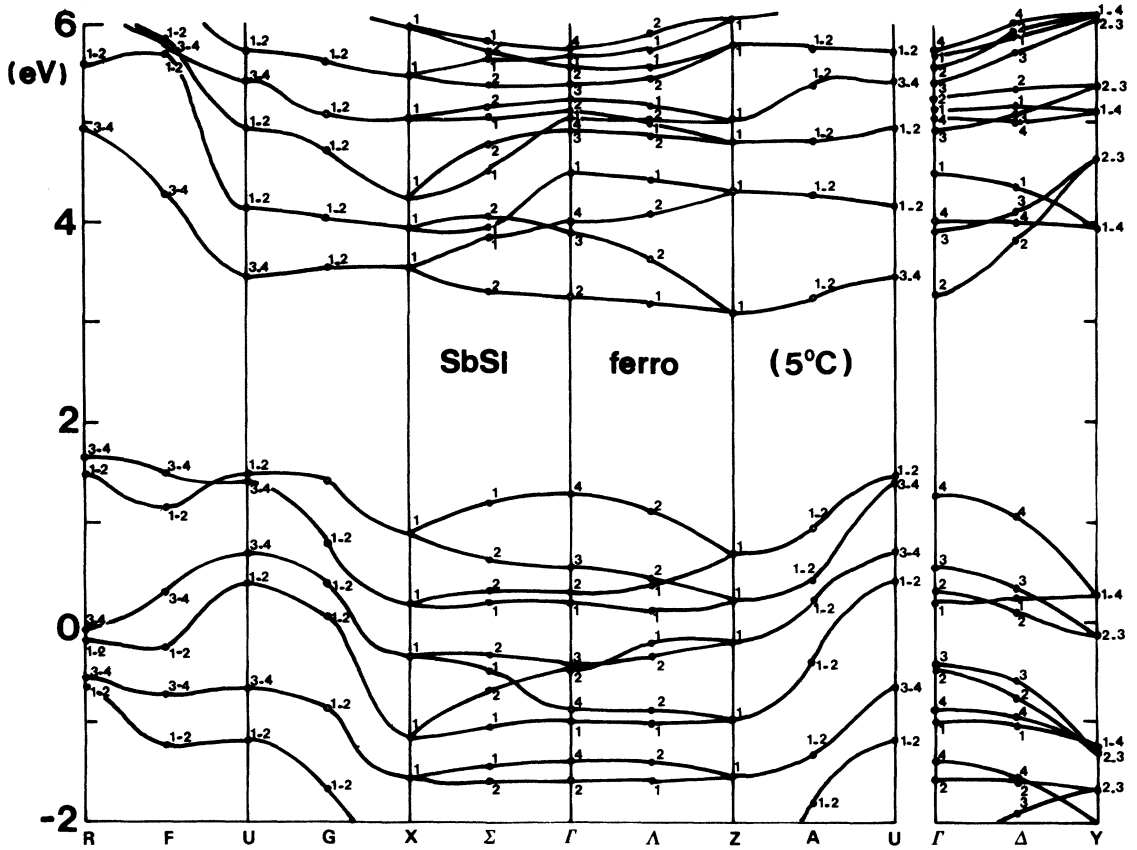

FIG. 6. Band structure of SbSI around the forbidden gap in the forroelectric phase. (The atomic positions at 5 °C are used in the calculation.) The numbers represent the corresponding irreducible representations at the symmetry points and lines.

$$T = (\hbar^2/2m)(\vec{K}+\vec{k})^2 = 1.504G \text{ eV}, \tag{21}$$

$$G = 1.37(h_x+p_x)^2 + 5.90(h_y+p_y)^2 + 0.974(h_z+p_z)^2, \tag{22}$$

where the set of h_x, h_y, and h_z is defined in Eq. (3) and the set of p_x, p_y, and p_z designates the wave vector $\vec{k}$ in the first Brillouin zone ($-\frac{1}{2} < p_x, p_y, p_z \leq \frac{1}{2}$). The above-mentioned band calculations have been made for $G = 50$. Thus the accuracy of the band energies is about 0.1 eV, but may be about 0.05 eV for the pair band.

The density of states of the bands is given by

$$D(E) = 2\sum_k \sum_i \delta(E_i(\vec{k}) - E), \tag{23}$$

where $E_i(\vec{k})$ is the energy of the ith band at the point $\vec{k}$. For the calculation of $D(E)$, the first Brillouin zone has been divided into 512 sections and the band structures have been calculated for the central points of each section. (Actually only 64 sections are needed, because the first Brillouin zone can be divided into 8 equivalent parts.) This number of sections is small compared with that usually taken for Ge, Si, etc.,[26] but it is expected that for the case of SbSI the calculated result will reveal the significant structures in $D(E)$ because all the bands of SbSI are very flat. The band calculations for the general $\vec{k}$ points have been made for $G = 40$. This means that the calculated accuracy of the energies is about 0.2 eV. Next the δ function in Eq. (23) has been approximated as

$$\delta(E_i(\vec{k}) - E) = \Delta(E_i(\vec{k}) - E), \tag{24}$$

$$\Delta(E_i(\vec{k}) - E) = 1 \text{ for } |E_i(\vec{k}) - E| \leq \tfrac{1}{2}\Delta E$$
$$= 0 \text{ for } |E_i(\vec{k}) - E| > \tfrac{1}{2}\Delta E. \tag{25}$$

The value of ΔE has been chosen to be 0.2 eV. The calculated result of $D(E)$ for the paraelectric phase is given by Fig. 8. As expected, this result shows many structures. It is found that the valence bands separate into five groups. As will be seen later, these are interpreted as the 5s-like bands of I atoms, the 3s-like bands of S atoms, the 5s-like bands of Sb atoms, the 5p-like bands of I atoms, and the 3p-like bands of S atoms as the energy increases. Similarly, the low-lying group of the conduction bands in Fig. 8 corresponds to the 5p-like bands of the Sb atoms. Further, it is seen

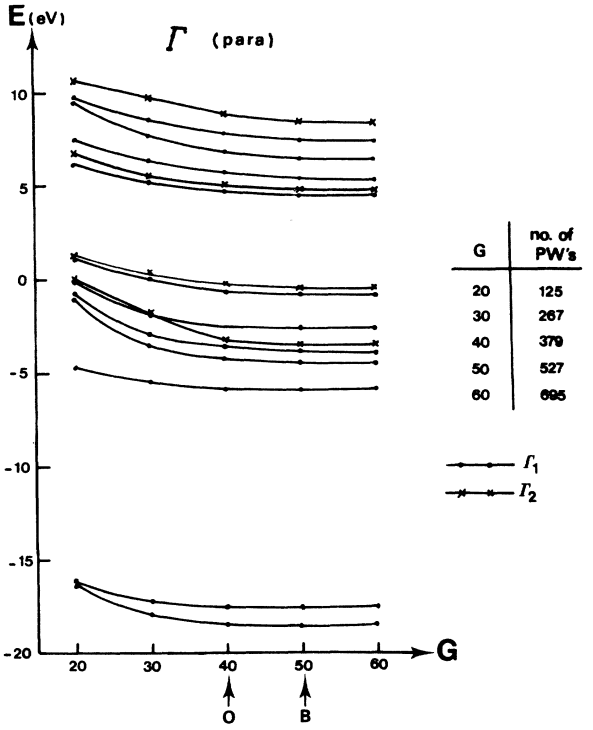

FIG. 7. Example of the convergence of the band energies. The quantity G represents the number of the plane waves employed in the band calculations. The symbols B and 0 show that the actual calculations of the band structures and of the dielectric constants and the density of states are made for $G=50$ and $G=40$, respectively.

that a dense concentration of many conduction bands exists in the higher-energy range.

Next, the character of each band has been qualitatively identified from the chemical point of view. For this purpose, the energy changes of each band have been calculated against the changes of the atomic form factors of each atom of SbSI. The example of the Γ_1 and Γ_2 states in the paraelectric phase is given in Fig. 9, where case 0 corresponds to the energy levels for the atomic form factors f of Fig. 3. Cases 1 and 3 represent the energy levels for the 10% increase of the values of the potential parameters A_α and B_α in Eq. (19) from case 0 for only the Sb and I atoms, respectively; case 2 represents those for the 10% decrease of the values of the corresponding quantities for only the S atom. It is found from this figure that only the specific bands change their positions greatly compared with the corresponding changes of the atomic form factors, which are indicated by the arrows in this figure. This tendency of the energy changes is seen to correspond to the changes of the atomic form factors, as the increase of the quantities A_α and B_α augments the negative part of $v_\alpha(\kappa)$, which means that the negative part of the atomic pseudopotential localizes more closely to the nucleus, and thus the energy levels become deep. From the results shown in Fig. 9, as well as the LCAO bases given in Table IV and the ionization energies of the atomic levels of each atom of SbSI, it is concluded that the character of each state is the following: 5s-like of I, 3s-like of S, 5s-like of Sb, 5p-like of I, 3p-like of S and 5p-like of Sb as the energy increases. These identifications are not, of course, exact, but they may indicate that the ionic model $Sb^{3+}S^{2-}I^{-}$ is profitable.

The difference in the ionicities of the Sb atom

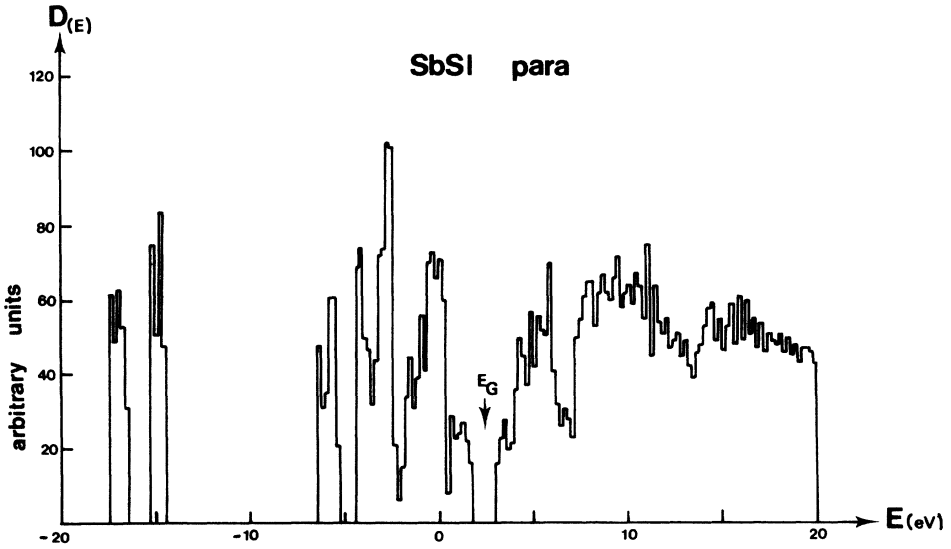

FIG. 8. Calculated density of states of the energy bands of SbSI in the paraelectric phase. The forbidden gap is shown by E_G.

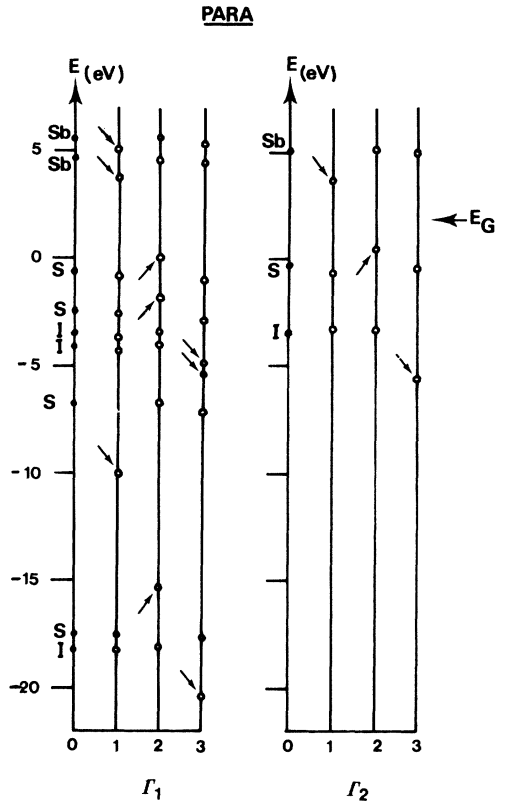

FIG. 9. Energy changes of the Γ_1 and Γ_2 states in the paraelectric phase against the changes of the atomic form factors of each atom of SbSI. The case 0 represents the energy levels for the atomic form factors f. The case 1, 2, and 3 represents those for the atomic form factors, whose potential parameters A_α and B_α of only the Sb, S, or I atoms are changed by 10% from the case 0, respectively. The arrows indicate the levels which move greatly against these changes of the atomic form factors. The forbidden gap is shown by E_G.

between SbSI and GaSb—that is, Sb^{3+} in SbSI and Sb^{3-} (or probably Sb^-) in GaSb—may raise some doubt about the potentials of the Sb atom to be used. In SbSI the electronegativities of S and I are larger than that of Sb, while the electronegativity of Ga is smaller than that of Sb. An uncertainty in the potential of the Sb atom may arise from the fact that the potentials of the Sb atom have, at present, been determined only for the Sb crystal and III-V compounds such as GaSb.

Then it is interesting to examine the low-lying s-like valence bands which are shown in Fig. 10, because these bands are not free electronlike and the pseudopotential method is thought of as less favorable to this case. The calculated results of Fig. 10 show, however, that the pseudopotential method gives reasonable band structures whose wave functions may be bound tightly to the atomic cores.[27] For these tightly localized states it is reasonable to assume that the interaction between two double chains of SbSI crystal is negligible.[7] This simplified one-double-chain model is characterized by its space group of C_{2h}^2. From the compatibility relation of C_{2h}^2 and D_{2h}^{16} given in Table IX, the $\Gamma_1-\Gamma_3$ states and the $\Gamma_6-\Gamma_8$ states are found to be accidentally degenerate in the simplified C_{2h}^2 model. This accidental degeneracy is seen for the 3s-like bands of the S atom in Fig. 10 and the simplified model is not as good for the 5s-like bands of the I and Sb atoms.

In order to investigate the optical properties of SbSI, the imaginary parts of the dielectric constant have been calculated for the paraelectric phase. (The calculation has not been made for the ferroelectric phase because in this case the atomic-structure constants are not real and this doubles the dimension of the matrix, which must be diagonalized in the calculation of band energies and wave functions.) The imaginary part of the dielectric constant is defined by

$$\epsilon_2^{(i)}(\omega)=\frac{8\pi^2e^2}{m^2\omega^2}\sum_{\vec{k}}\sum_{c,v}|\epsilon_i p_{cv}|^2 \times\delta(E_c(\vec{k})-E_v(\vec{k})-\hbar\omega), \tag{26}$$

where ϵ_i is the ith component of the unit polarization vector of the incident light with the energy $\hbar\omega$, and p_{cv} is the matrix element of the momentum operator between the empty-conduction and filled-valence bands, whose energies are given by $E_c(\vec{k})$ and $E_v(\vec{k})$. The index i of $\epsilon_2^{(i)}(\omega)$ corresponds to the polarization of the incident light. The method calculating of $\epsilon_2^{(i)}(\omega)$ is the same as that employed for the density of states. The first Brillouin zone has been divided into 512 sections and the band calculations for each section have been made for $G=40$, which corresponds to the accuracy of about 0.1 eV for the pair bands. The value of ΔE in the Δ function defined by Eq. (25) has been taken to be 0.1 eV.

The calculated $\omega^2\epsilon_2^{(i)}(\omega)$ of SbSI in the paraelectric phase is shown in Fig. 11 for three polarizations ($i=a$, b, or c for $\vec{E}\parallel\vec{a}$, $\vec{E}\parallel\vec{b}$, or $\vec{E}\parallel\vec{c}$). In these figures, the shaded part represents the contribution from the nonsymmetric (NS) sections, in which no symmetry points or lines of the Brillouin zone are contained. It is seen, first, that the dielectric constant is greatly dependent on the polarization. Second, there exist many fine structures at least within the precision of 0.1 eV. Third, the contribution from the NS part has almost the same structure as the total $\epsilon_2^{(i)}(\omega)$. The first feature is related to the anisotropic crystal structure of SbSI[25] and the second and third ones are the consequences of its band structures; that is, there are many close-energy levels over the whole Brillouin zone and the $\vec{k}$ dependence of each band is not large.

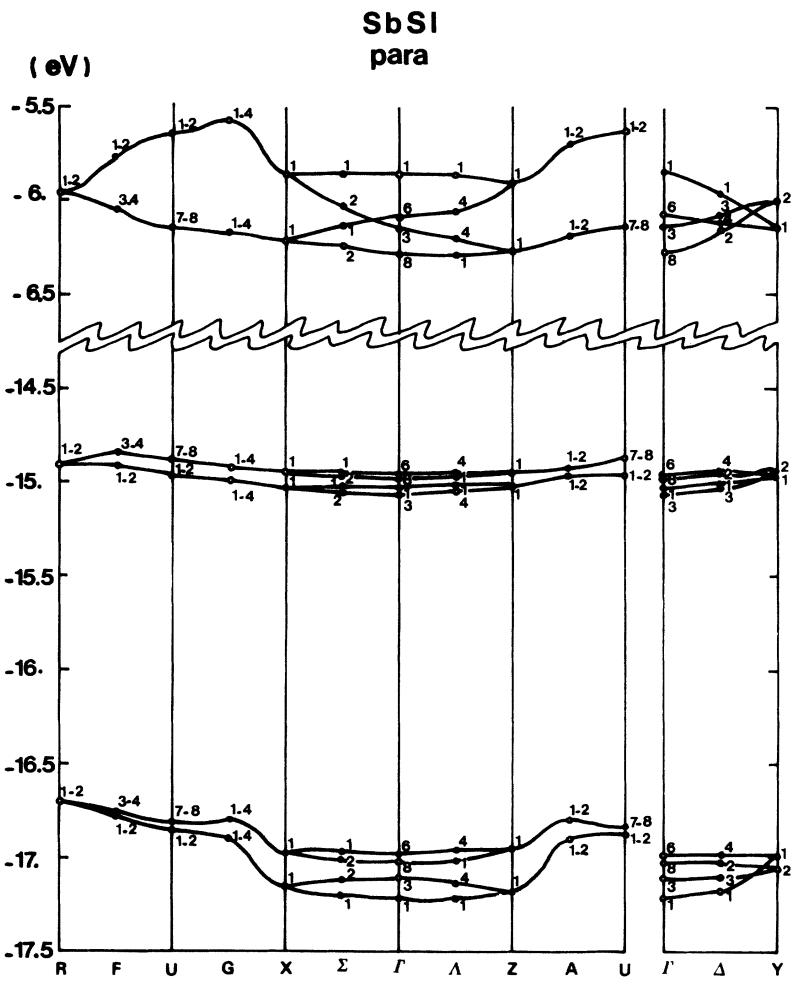

FIG. 10. Band structures of s-like valence bands of SbSI in the paraelectric phase. It should be noted that the energy scale of this figure is different from that of Fig. 5.

As described in Sec. V, the usual critical-point analysis of the structures in $\epsilon_2^{(i)}(\omega)$ is not meaningful, but the large peaks in $\epsilon_2^{(i)}(\omega)$ below 6 eV have been found to be due to the optical transitions to the low-lying group of the conduction band, which reveals the peak around 5 eV in the density of states (Fig. 8), while the peaks above 8 eV are due to the transitions to the higher-conduction bands. Finally, the decrease of the magnitude of $\epsilon_2^{(i)}(\omega)$ above 10 eV may be due to the exhaustion of the oscillar strengths of the valence bands.

V. DISCUSSION

A. Comparison with the Experiments Giving Optical Properties of SbSI

The calculated results of the band structures and the dielectric constants are first compared with the experimental results of the optical properties summarized in Sec. I.

(i) The values of the absorption edges of SbSI in the paraelectric phase have been used for the determination of the atomic form factors so as to obtain the correct values of the absorption edges for $\vec{E} \parallel \vec{c}$ and $\vec{E} \perp \vec{c}$. It should be only noted here that the values used for the absorption edges are not precise because the line shapes of the absorption edges have the Urbach tail[28] and the gap energies cannot be determined with good precision from the experiments.

(ii) Use has been made of the similarity of the line shapes of the absorption edges in both the

TABLE IX. Character table of the group C_{2h} and the compatibility relation of C_{2h} and D_{2h}. (The definition of the symmetry operations is given in the Appendix.)

C_{2h}	E	$C_2^{(y)}$	I	$\sigma_v^{(xz)}$
Γ_1	1	1	1	1
Γ_2	1	−1	1	−1
Γ_3	1	1	−1	−1
Γ_4	1	−1	−1	1

D_{2h}	Γ_1	Γ_2	Γ_3	Γ_4	Γ_5	Γ_6	Γ_7	Γ_8
C_{2h}	Γ_1	Γ_3	Γ_1	Γ_3	Γ_2	Γ_4	Γ_2	Γ_4

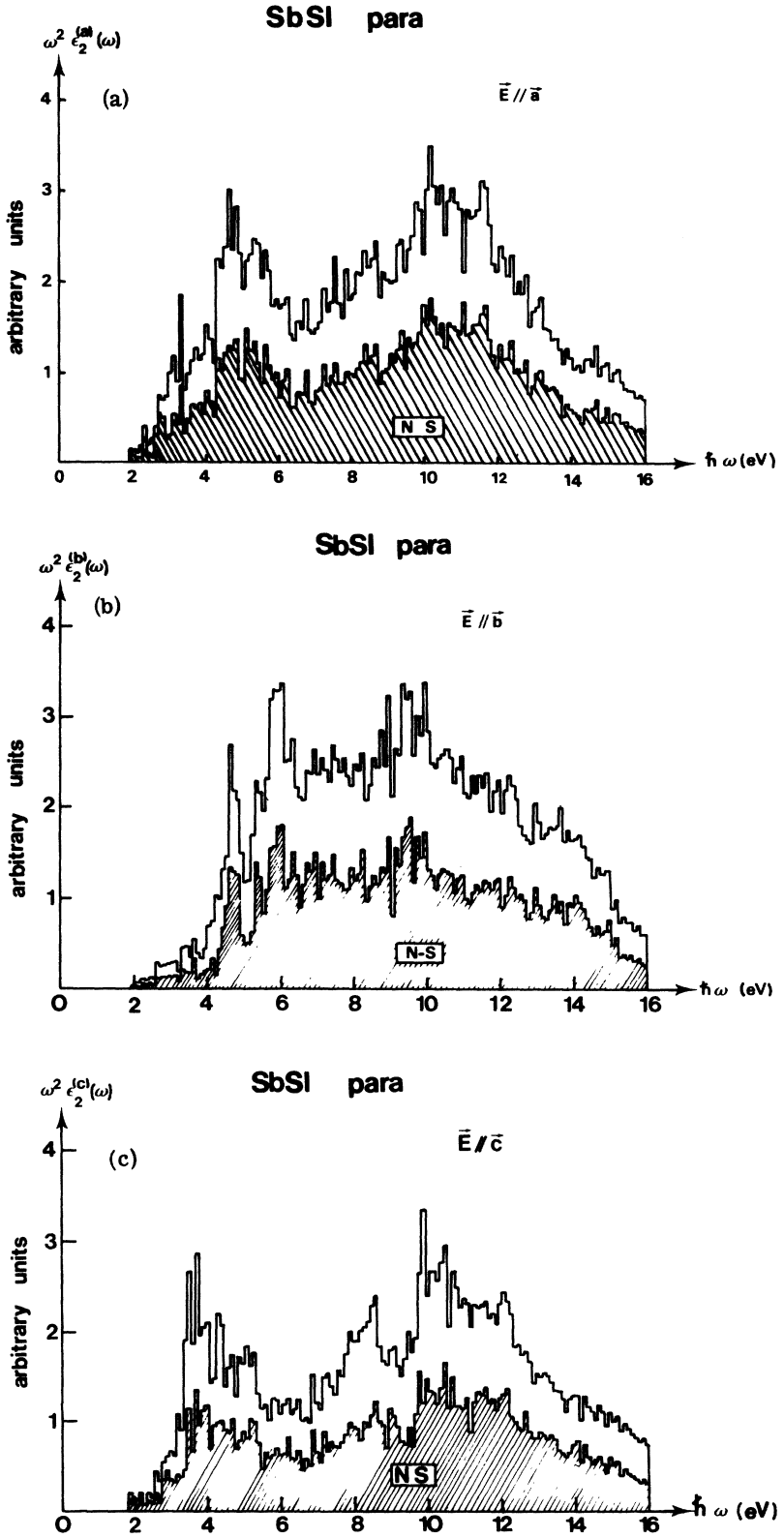

FIG. 11. Calculated imaginary parts of the dielectric constant of SbSI in the paraelectric phase for (a) $\vec{E} \| \vec{a}$, (b) $\vec{E} \| \vec{b}$, and (c) $\vec{E} \| \vec{c}$. The ordinate represents the quantity $\omega^2 \epsilon_2^{(i)}(\omega)$, where $i = a$, b, or c. The shaded part (NS) is the contribution from the sections which do not contain any symmetry points or lines of the Brillouin zone.

para- and ferroelectric phases, according to the assumption that the absorption edges of both phases are brought about by the optical transitions at the same critical point in the Brillouin zone. However, since the adjustment of the atomic form factors has been made only for the paraelectric phase, and the same atomic form factors have been employed for the ferroelectric phase, the calculated edges for the latter phase have the inverse dichroism to the observed one.[3,13] As for the over-all band structures, they are similar in both phases.

(iii) The calculated value of the edge shift between both phases is ± 0.13 eV, which is the average of the values for $\vec{E} \parallel \vec{c}$ and $\vec{E} \perp \vec{c}$; the measured value is about $+0.1$ eV.[3,14]

(iv) It has been initially assumed that the absorption edges correspond to direct transitions.

(v) The existence of an indirect absorption below the direct edges is in agreement with the calculated result that SbSI has an indirect gap in both phases.

(vi) The resemblance of the observed reflectivities of both phases is the consequence of the resemblance of the over-all band structures in both phases.

(vii) The calculated dielectric constants for three polarizations show many fine structures which may give rise to the fine structures in the reflectivities. There is also in Figs. 11 and 12 clear difference in reflectance between $\vec{E} \parallel \vec{c}$ and $\vec{E} \perp \vec{c}$; this difference is due to the differences in the dipole-matrix elements. The dipole-matrix element for $\vec{E} \parallel \vec{c}$ is greater than that for $\vec{E} \perp \vec{c}$, between 2 and 4 eV, where measurements are available.[16]

(viii) An experimentally determined dielectric constant[12] has been determined for the case of $\vec{E} \parallel \vec{c}$ only in the paraelectric phase. For comparison with this experimental result, the phenomenological broadening factor γ has been introduced into the calculation in order to diminish the fine structure in the calculated $\epsilon_2^{(\vec{1})}(\omega)$. This has been done by replacing the Δ function in Eq. (25) by the following Lorentzian function:

$$f(E_c(\vec{k}) - E_v(\vec{k}) - \hbar\omega) = \frac{\Delta E}{\pi} \frac{\gamma}{[E_c(\vec{k}) - E_v(\vec{k}) - \hbar\omega]^2 + \gamma^2} . \tag{27}$$

The value of γ has been chosen to be 0.1 eV. The calculated results of $\omega^2 \epsilon_2^{(i)}(\omega)$ are given by the solid curves in Fig. 12, as are the above-mentioned experimental results, which are shown by the dashed curve. Below 6 eV there are five structures in both the calculated and experimental curves. These structures are marked by the arrows in Fig. 12 and listed in Table X, where the critical points at which the transitions give rise to the corresponding structure are summarized. For the higher

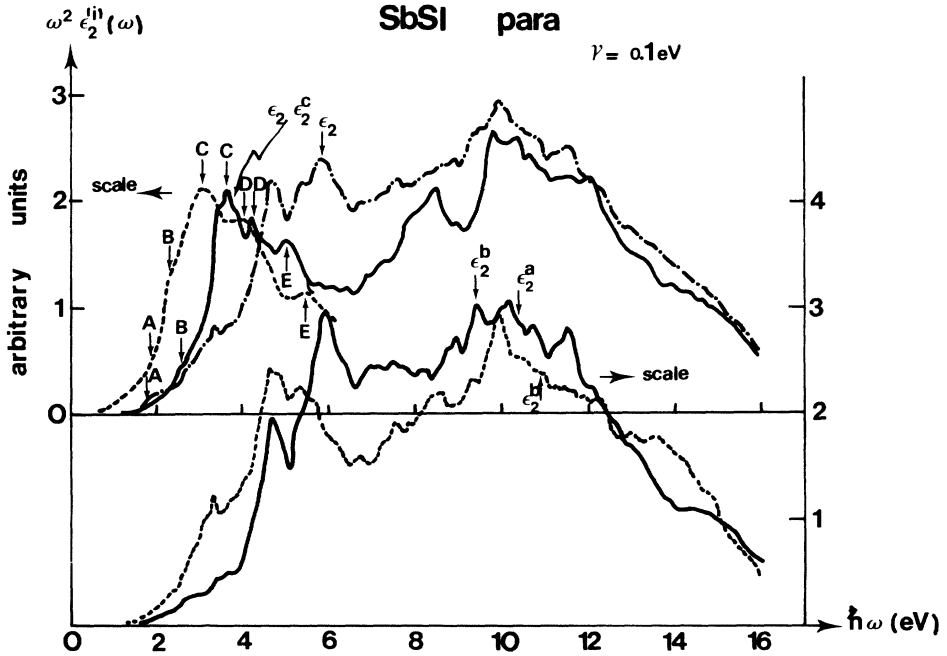

FIG. 12. Imaginary parts of the dielectric constant with the phenomenological broadening factor $\gamma = 0.1$ eV. The solid curves $\epsilon_2^{\parallel}$ and $\epsilon_2^{\perp}$ show the calculated dielectric constants for $\vec{E} \parallel \vec{c}$ and $\vec{E} \perp \vec{c}$, where $\epsilon_2^{\perp}$ is the average for $\epsilon_2^{(a)}$ and $\epsilon_2^{(b)}$. The dashed curve is the experimental curve for $\vec{E} \parallel \vec{c}$ cited by Nikiforov and Khasabov (Ref. 12). The five structures seen in the dielectric constants for $\vec{E} \parallel \vec{c}$ below 6 eV are marked by the arrows.

TABLE X. Observed and calculated positions of the structures in the imaginary part of the dielectric constant of SbSI in the paraelectric phase for $\vec{E} \parallel \vec{c}$.

Structure	Position expt.[a]	Position cal.	Critical points at which the transitions contribute to the corresponding structure
A (kink)	1.9 eV	1.8 eV	*U*
B (hump)	2.3	2.5 (?)	
C (peak)	3.1	3.6	*U Σ A G D*
D (peak)	4.0	4.3	*Γ X U R Σ Δ Λ A G F B*
E (peak)	5.5	5.0	*T Σ Δ G F B E*

[a] This value is taken from the figure cited by Nikiforov and Khasabov (Ref. 12).

three peaks, the agreement is not as bad for their positions and relative magnitudes. Finally it should be remarked that each structure is brough about at many critical points and thus the usual critical-point analysis of the structures in the dielectric constants is not meaningful for SbSI.

B. Correlation of Band Structures with the Ferroelectric Phase Transition

Next, the band structures of SbSI in both the para- and ferroelectric phases are compared to each other in order to study the effect of the spontaneous polarization in the ferroelectric phase on the band structures. In Table XI the calculated energies of several bands and pair bands are listed for both phases. It is seen from this table that the change of energy values is very dependent on the states and that the energy values of the states at the *U* and *R* points greatly change from the para- to the ferroelectric phases. This fact as well as the fact that the states at these points are considerably sensitive to the pseudopotentials (Fig. 4) may show that the ferroelectric phase transition is related to the instability of the electronic states in addition to the instability of the lattice.[29]

From Table XI, the polarization potentials described in Sec. III can be easily obtained by the use of the measured value[1] of the spontaneous polarization at 5 °C of $P_s = 0.19$ C/m^2. The results are given in Table XII. The magnitude of the calculated polarization potentials is of the same order as those obtained by Zook and Casselman[30] for $SrTiO_3$. Strictly speaking, the values of the polarization potential given in Table XII also include the effect of the change of the lattice constants. However, the change of the lattice constants between the two phases is very small, so that the calculated changes of the energy levels between both phases can be considered mainly as the effect of the polarization, although the observed temperature dependence of the absorption edge ($dE_G/dT = -0.9 \times 10^{-3}$ eV/°K) in the paraelectric phase may be due to the effect of the change of the lattice constants. In this connection, the large temperature dependence of the absorption edge ($dE_G/dT = -2.2 \times 10^{-3}$ eV/°K) observed in the ferroelectric phase for $\vec{E} \perp \vec{c}$ can be treated in terms of the polarization potential. In practice, substituting the value of $b(U_{7-8}^{(c)} - U_{1-2}^{(v)}) = 1.7\,\mathrm{eV\,m^4/C^2}$ and the observed relation such as $P_S^2 = -20 \times 10^{-4}(T - T_0)$ C^2/m^4 into Eq. (15), one obtains the temperature dependence of the absorption edge for $\vec{E} \perp \vec{c}$ as follows: $dE_G/dT = -3.4 \times 10^{-3}$ eV/°K. This value is thought of as good if the inaccuracy of the band calculation is taken into account.

The electro-optic effects of the absorption edges are calculated with the use of these polarization potentials. Under the assumption that the electric susceptibilities are the same for both phases, the following relation can be obtained from Eqs. (17) and (18):

$$\Delta E_G^{(f)2} / \Delta E_G^{(p)} = 4bP_s^2(T). \tag{28}$$

TABLE XI. Calculated energy values of several bands and pair bands of SbSI in the para- and ferroelectric phases. The unit is eV.

Para (35 °C)		Ferro (5 °C)		
Band[a]	*E*(para)	Band[a]	*E*(ferro)	*E*(ferro)-*E*(para)[b]
$\Gamma_6^{(v)}$	1.28	$\Gamma_4^{(v)}$	1.29	0.01
$\Gamma_3^{(v)}$	0.40	$\Gamma_3^{(v)}$	0.55	0.15
$\Gamma_8^{(c)}$	3.30	$\Gamma_2^{(c)}$	3.27	−0.03
$\Gamma_6^{(c)}$	3.92	$\Gamma_4^{(c)}$	3.97	0.07
$\Gamma_3^{(c)}$	3.96	$\Gamma_3^{(c)}$	3.90	−0.06
$X_1^{(v)}$	0.81	$X_1^{(v)}$	0.88	0.07
$X_1^{(c)}$	3.57	$X_1^{(c)}$	3.57	0.0
$Y_1^{(v)}$	0.20	$Y_{1-4}^{(v)}$	0.27	0.07
$Y_1^{(c)}$	3.97	$Y_{1-4}^{(c)}$	3.96	−0.01
$Z_1^{(v)}$	0.64	$Z_1^{(v)}$	0.66	0.02
$Z_1^{(c)}$	3.10	$Z_1^{(c)}$	3.08	−0.02
$U_{5-6}^{(v)}$	1.69	$U_{3-4}^{(v)}$	1.42	−0.27
$U_{1-2}^{(c)}$	1.60	$U_{1-2}^{(v)}$	1.48	−0.12
$U_{7-8}^{(c)}$	3.51	$U_{3-4}^{(c)}$	3.45	−0.06
		$R_{3-4}^{(v)}$	1.65	0.36[c]
$R_{1-2}^{(v)}$		$R_{1-2}^{(v)}$	1.48	
		$R_{3-4}^{(c)}$	4.94	0.33[c]
$R_{1-2}^{(c)}$		$R_{1-2}^{(c)}$	5.60	
$\Gamma_8^{(c)} - \Gamma_6^{(v)}$	2.02	$\Gamma_2^{(c)} - \Gamma_4^{(v)}$	1.98	−0.04
$U_{7-8}^{(c)} - U_{5-6}^{(c)}$	1.82	$U_{3-4}^{(c)} - U_{3-4}^{(v)}$	2.03	0.21
$U_{7-8}^{(c)} - U_{1-2}^{(v)}$	1.91	$U_{3-4}^{(c)} - U_{1-2}^{(v)}$	1.97	0.06
$R_{1-2}^{(c)} - R_{1-2}^{(v)}$	3.74	$R_{3-4}^{(c)} - R_{3-4}^{(v)}$ $R_{1-2}^{(c)} \quad R_{1-2}^{(v)}$	3.71	−0.03[c]

[a] The indices *v* and *c* indicate the valence and conduction bands, respectively.

[b] This value is the energy difference of the states in both phases which are connected each other by the compatibility relation between two phases.

[c] This value is calculated with the use of the averaged energy of the two states at the *R* point in the ferroelectric phase.

TABLE XII. Polarization potentials for several bands and pair-bands. (The unit is eV m^4/C^2.)

$b(\Gamma_6^{(v)})$	0.3
$b(\Gamma_8^{(c)})$	−0.9
$b(U_{5-6}^{(v)})$	−7.8
$b(U_{1-2}^{(v)})$	−3.5
$b(U_{7-8}^{(c)})$	−1.7
$b(\Gamma_8^{(c)}-\Gamma_6^{(v)})$	−1.2
$b(U_{7-8}^{(c)}-U_{5-6}^{(v)})$	6.1
$b(U_{7-8}^{(c)}-U_{1-2}^{(v)})$	1.7

For $\vec{E} \parallel \vec{c}$, the quantity b in this equation is $b(U_{7-8}^{(c)} - U_{5-6}^{(v)})$ in Table XII, because the absorption edge exists at the U point. The value of Eq. (28) is calculated as 2.9×10^{-1} eV by using the value of $b(U_{7-8}^{(c)} - U_{5-6}^{(v)}) = 6.1\,\mathrm{eV\,m^4/C^2}$ and the observed value[1] of $P_s^2(T = 16.6\,^\circ\mathrm{C}) = 120\times10^{-4}\,\mathrm{C^2/m^4}$, whereas the corresponding value obtained from the measured electro-optic effect is 2.9×10^{-3} eV, where the observed values[13] are used for $\Delta E_G^{(f)} = 3.3\times10^{-3}$ eV (at 16.6 °C) and $\Delta E_G^{(p)} = 3.8\times10^{-3}$ eV (at 25.5 °C) at $E_{ext} = 1$ kV/cm. Thus the calculated value is much greater than the observed one. This discrepancy is now unaccountable, because the calculated value of the edge shift between both phases is in agreement with the experiment.

The discussion given in this paragraph is not completely correct, because the temperature dependence of χ in Eqs. (17) and (18) has not been taken into account. The quantity χ can be related to the static dielectric constant as follows:

$$\chi = [\epsilon_S(T) - 1]/4\pi .$$

Then Eq. (28) should be written

$$\Delta E_G^{(f)2}/\Delta E_G^{(p)} = 4b[\epsilon_S(T^{(f)})/\epsilon_S(T^{(p)})]^2 P_S(T^{(f)}), \quad (28)$$

where $T^{(f)}$ and $T^{(p)}$ represent the temperatures considered in the ferro- and paraelectric phases, respectively. Using the measured values of $\epsilon_S(T^{(f)} = 16.6\,^\circ\mathrm{C}) = 3.1\times10^3$ and of $\epsilon_S(T^{(p)} = 25.5\,^\circ\mathrm{C}) = 14.3\times10^3$, one obtains the value of Eq. (28) as 1.3×10^{-2} eV. Thus the calculated value is greater than the observed one only by a factor of 4. This discrepancy may be due to the large elongation of the crystal under the external electric field ($dc/c/dE = 3.5\times10^{-7}$/V/cm).

C. General Features of Band Structures of the Complex Crystals

From the calculations of the band structures and optical properties of SbSI, the following features are deduced as the characteristics of the complex crystals: (i) the existence of many close-energy levels, (ii) the small bandwidth or the large effective mass, (iii) the existence of a fine structure in the dielectric constants or in the reflectivity, and (iv) the fact that many $\vec{k}$ points in the Brillouin zone contribute almost equally to the structures of the optical constants or, in other words, it is not necessary to use the usual critical-point analysis.

D. Discussion of Obtained Pseudopotentials and Comparison of Calculated Band Structures with Other Band Calculations of SbSI

Although the calculated band structures of SbSI explain fairly well the existing experimental results, there exists much uncertainty regarding the obtained atomic form factors. In particular, the atomic form factor of the I atom has been chosen arbitrarily to some extent, because this has been primarily determined from that of the Cl atom and the band structures around the forbidden gap did not depend strongly on this form factor. The precise determination of this form factor must be done by the comparison with the experiments of the optical properties of higher-energy range. The problem exists, however, in the atomic form factor of the S atom rather than that of the I atom, because the values of $v_S(\kappa)$ obtained up to the present for other crystals scatter widely, as seen in Fig. 3(b).

The calculated results for the ferroelectric phase show poorer agreement with the experiments than those for the paraelectric phase. One of the reasons for this is that the same atomic form factors have been used for both phases. If the atomic form factors are different in both phases, it is very interesting because the polarization of core electrons may contribute largely to the spontaneous polarization.

The calculations have been made by the use of the values of the atomic positions at 5 and 35 °C, but the effects of the lattice vibrations have not been considered. One of these effects may be included directly in the band calculations by multiplying the atomic structure factors by the Debye-Waller factors, as was done for PbTe and SnTe by Tsang and Cohen.[31] Further, the electron-phonon interaction will affect the band structures near the ferroelectric phase transition because this interaction plays an important role in the phase transition of the displacive-type ferroelectric[29] such as SbSI.

Next it should be pointed out that, simply from the symmetry point of view, the absorption edges of SbSI may exist on the symmetry lines Δ or F, as shown in Sec. II. Although the bottom of the conduction band has been supposed to be on the Δ lines by Bercha *et al.*,[16] this possibility seems unlikely within the calculated results described in the previous sections.

The band structures and optical properties of SbSI have been also investigated by Yamada and

TABLE XIII. Characters of the irreducible representations of the group $\vec{k}$ of D_{2h}^{16}.

	E	$C_2^{(x)}$	$C_2^{(y)}$	$C_2^{(z)}$	I	$\sigma_v^{(yz)}$	$\sigma_v^{(xz)}$	$\sigma_v^{(xy)}$
Γ_1	1	1	1	1	1	1	1	1
Γ_2	1	1	1	1	−1	−1	−1	−1
Γ_3	1	−1	1	−1	1	−1	1	−1
Γ_4	1	−1	1	−1	−1	1	−1	1
Γ_5	1	1	−1	−1	1	1	−1	−1
Γ_6	1	1	−1	−1	−1	−1	1	1
Γ_7	1	−1	−1	1	1	−1	−1	1
Γ_8	1	−1	−1	1	−1	1	1	−1
X_1	2	0	0	0	0	0	2	0
X_2	2	0	0	0	0	0	−2	0
Y_1	2	0	0	0	0	0	0	2
Y_2	2	0	0	0	0	0	0	−2
Z_1	2	0	0	0	0	0	2	0
Z_2	2	0	0	0	0	0	−2	0
R_1	2	0	0	0	0	0	0	$2i$
R_2	2	0	0	0	0	0	0	$-2i$
S_1	2	$2i$	0	0	0	0	0	0
S_2	2	$-2i$	0	0	0	0	0	0
T_1	2	2	0	0	0	0	0	0
T_2	2	−2	0	0	0	0	0	0
U_1	1	i	1	i	1	i	1	i
U_2	1	$-i$	1	$-i$	1	$-i$	1	$-i$
U_3	1	i	1	i	−1	$-i$	−1	$-i$
U_4	1	$-i$	1	$-i$	−1	i	−1	i
U_5	1	i	−1	$-i$	1	i	−1	$-i$
U_6	1	$-i$	−1	i	1	$-i$	−1	i
U_7	1	i	−1	$-i$	−1	$-i$	1	i
U_8	1	$-i$	−1	i	−1	i	1	$-i$

	E	$C_2^{(x)}$	$C_2^{(y)}$	$C_2^{(z)}$	I	$\sigma_v^{(yz)}$	$\sigma_v^{(xz)}$	$\sigma_v^{(xy)}$
Σ_1	1	α					1	α
Σ_2	1	$-\alpha$					1	$-\alpha$
Σ_3	1	α					−1	$-\alpha$
Σ_4	1	$-\alpha$					−1	α
	The group of A, C, and E are equivalent to the group of Σ.							
Δ_1	1		β			β		1
Δ_2	1		$-\beta$			β		−1
Δ_3	1		β			$-\beta$		−1
Δ_4	1		$-\beta$			$-\beta$		1
B_1	2		0			0		0
D_1	2		0			0		0
F_1	1		β			$i\beta$		i
F_2	1		β			$-i\beta$		$-i$
F_3	1		$-\beta$			$i\beta$		$-i$
F_4	1		$-\beta$			$-i\beta$		i
Λ_1	1			γ		γ	1	
Λ_2	1			$-\gamma$		γ	−1	
Λ_3	1			γ		$-\gamma$	−1	
Λ_4	1			$-\gamma$		$-\gamma$	1	
	The group of G is equivalent to the group of Λ.							
H_1	2			0		0	0	
	The group of Q is equivalent to the group of H.							

$\alpha = e^{\pi i p_x}$ $(-\frac{1}{2} < p_x < \frac{1}{2})$, $\beta = e^{\pi i p_y}$ $(-\frac{1}{2} < p_y < \frac{1}{2})$, $\gamma = e^{\pi i p_z}$ $(-\frac{1}{2} < p_z < \frac{1}{2})$

The following pairs of states are degenerate each other by TR:

$R_1 - R_2$; $S_1 - S_2$; $U_1 - U_2$, $U_3 - U_4$, $U_5 - U_6$, $U_7 - U_8$;
$A_1 - A_2$, $A_3 - A_4$; $C_1 - C_4$, $C_2 - C_3$; $E_1 - E_3$, $E_2 - E_4$;
$F_1 - F_2$, $F_3 - F_4$; $G_1 - G_4$, $G_2 - G_3$; $2Q_1$.

Chihara[10] and Nikiforov and Khasabov[12] using the LCAO method for the simplified one-double-chain model described in Sec. IV. Since this simplified model is not useful for SbSI except for the deep s-like bands, the precise comparison of the calculated results with the above-mentioned calculations cannot be made, but the over-all band structures are similar. Furthermore, the dielectric constant calculated by Nikiforov and Khasabov[12] is not in good agreement with the experiment and does not show the large peak around 10 eV that exists in the calculated results of this work (Figs. 11 and 12). This peak is due to the conduction bands being constructed from states other than the atomic p states, as described in Sec. IV.

Thus, the calculated results of the band structures and the optical properties of SbSI in this work are sufficient for the moment. More experiments are necessary for more precise calculations and detailed comparison: In particular, the optical measurements of the absorption edges and of the reflectivities in the wide energy range for various polarizations of the incident light, as well as the temperature (or pressure) dependence of the optical properties and their electro-optic effects are desirable.

VI. CONCLUSIONS

In this work, the electronic band structures of SbSI have been calculated by the pseudopotential method in the para- and ferroelectric phases. Although the atomic form factors have not been determined precisely for the moment, the calculated band structures explain the experiments fairly well. The SbSI crystal has an indirect gap in both phases and has the smallest direct gap at the U point. This direct gap brings about the dichroism in the absorption edge. The over-all band struc-

TABLE XIV. Characters of the irreducible representations of the group $\vec{k}$ of C_{2v}^9.

	E	$C_2^{(y)}$	$\sigma_v^{(yz)}$	$\sigma_v^{(xy)}$
Γ_1	1	1	1	1
Γ_2	1	−1	1	−1
Γ_3	1	1	−1	−1
Γ_4	1	−1	−1	1
X_1	2	0	0	0
Y_1	1	i	i	1
Y_2	1	$-i$	i	−1
Y_3	1	i	$-i$	−1
Y_4	1	$-i$	$-i$	1
Z_1	2	0	0	0
R_1	1	i	−1	i
R_2	1	i	1	$-i$
R_3	1	$-i$	−1	$-i$
R_4	1	$-i$	1	i
S_1	2	0	0	0
T_1	2	0	0	0
U_1	1	1	i	i
U_2	1	1	$-i$	$-i$
U_3	1	−1	i	$-i$
U_4	1	−1	$-i$	i

$\alpha = e^{\pi i p_x}$ $(-\frac{1}{2} < p_x < \frac{1}{2})$
$\beta = e^{\pi i p_y}$ $(-\frac{1}{2} < p_y < \frac{1}{2})$
$\gamma = e^{\pi i p_z}$ $(-\frac{1}{2} < p_z < \frac{1}{2})$

	E	$C_2^{(y)}$	$\sigma_v^{(yz)}$	$\sigma_v^{(xy)}$
Σ_1	1			α
Σ_2	1			α

The group of A, C, and E is equivalent to the group of Σ.

Δ_1	1	β	β	1
Δ_2	1	$-\beta$	β	−1
Δ_3	1	β	$-\beta$	−1
Δ_4	1	$-\beta$	$-\beta$	1
B_1	2	0	0	0
D_1	2	0	0	0
F_1	1	β	$i\beta$	i
F_2	1	β	$-i\beta$	$-i$
F_3	1	$-\beta$	$i\beta$	$-i$
F_4	1	$-\beta$	$-i\beta$	i
Λ_1	1		γ	
Λ_2	1		$-\gamma$	

The group of G is equivalent to the group of Λ.

H_1	1		$i\gamma$	
H_2	1		$-i\gamma$	

The group of Q is equivalent to the group of H.

The following pairs of states are degenerate each other by TR:

$Y_1 - Y_4$, $Y_2 - Y_3$; $R_1 - R_2$, $R_3 - R_4$; $U_1 - U_2$, $U_3 - U_4$; $A_1 - A_2$; $2C_1$, $2C_2$; $E_1 - E_2$; $F_1 - F_2$, $F_3 - F_4$; $H_1 - H_2$; $Q_1 - Q_2$.

tures in both phases are similar, but the absorption edge has a shift of about 0.1 eV from the para- to the ferroelectric phases. The band's density of states is very large and has several peaks. As for the correlation of the band structures with the ferroelectric phase transition, some bands change their energy values greatly at the phase transition. The dielectric constant has also been calculated in the paraelectric phase and it has been shown that this is strongly dependent on the polarization of the incident light. The agreement with the existing experimental result is satisfactory. Further, several characteristics of the band structures in complex crystals have been deduced from this work on SbSI.

TABLE XV. Compatibility relations of D_{2h}^{16}.

Γ_1	Γ_2	Γ_3	Γ_4	Γ_5	Γ_6	Γ_7	Γ_7	X_1	X_2	Y_1	Y_2
Σ_1	Σ_3	Σ_2	Σ_4	Σ_3	Σ_1	Σ_4	Σ_2	$\Sigma_1+\Sigma_2$	$\Sigma_3+\Sigma_4$	C_1+C_4	C_2+C_3
Δ_1	Δ_3	Δ_3	Δ_1	Δ_2	Δ_4	Δ_4	Δ_2	D_1	D_1	$\Delta_1+\Delta_4$	$\Delta_2+\Delta_3$
Λ_1	Λ_3	Λ_4	Λ_2	Λ_2	Λ_4	Λ_3	Λ_1	G_1+G_4	G_2+G_3	H_1	H_1

Z_1	Z_2	R_1	R_2	S_1	S_2	T_1	T_2
A_1+A_2	A_3+A_4	E_1+E_4	E_2+E_3	C_1+C_3	C_2+C_4	E_1+E_3	E_2+E_4
B_1	B_1	F_1+F_4	F_2+F_3	D_1	D_1	B_1	B_1
$\Lambda_1+\Lambda_4$	$\Lambda_2+\Lambda_3$	Q_1	Q_1	Q_1	Q_1	H_1	H_1

U_1	U_2	U_3	U_4	U_5	U_6	U_7	U_8
A_1	A_2	A_3	A_4	A_3	A_4	A_1	A_2
F_1	F_2	F_2	F_1	F_3	F_4	F_4	F_3
G_1	G_4	G_3	G_2	G_2	G_3	G_4	G_1

TABLE XVI. Compatibility relations of C_{2v}^9.

Γ_1	Γ_2	Γ_3	Γ_4	X_1	Y_1	Y_2	Y_3	Y_4	Z_1
Σ_1	Σ_2	Σ_2	Σ_1	$\Sigma_1+\Sigma_2$	C_1	C_2	C_2	C_1	A_1+A_2
Δ_1	Δ_2	Δ_3	Δ_4	D_1	Δ_1	Δ_2	Δ_3	Δ_4	B_1
Λ_1	Λ_1	Λ_2	Λ_2	G_1+G_2	H_1	H_1	H_2	H_2	$\Lambda_1+\Lambda_2$

R_1	R_2	R_3	R_4	S_1	T_1		U_1	U_2	U_3	U_4
E_1	E_2	E_2	E_1	C_1+C_2	E_1+E_2		A_1	A_2	A_2	A_1
F_1	F_2	F_3	F_4	D_1	B_1		F_1	F_2	F_3	F_4
Q_1	Q_2	Q_1	Q_2	Q_1+Q_2	H_1+H_2		G_1	G_2	G_1	G_2

Thus the calculations described in the previous sections are sufficient for the first trial of the quantitative band calculations of SbSI. For further development, many precise experiments are necessary. The measurements of the reflectivity in wide energy range as well as more precise calculations of the band structure will appear in the near future.

Finally, it is shown through this work that the pseudopotential method is suitable for the band calculations of complex crystals and also of ionic crystals.[25]

ACKNOWLEDGMENTS

The authors would like to express their thanks to Professor M. L. Cohen for the useful comments. One of them (K. N.) wishes also to thank Professor H. Kamimura for the helpful discussion in the early stage of this work.

APPENDIX

The symmetry operations of D_{2h}^{16} (paraelectric phase) are as follows (the translational symmetry operations being excluded):

$$\begin{aligned} &\{E \mid 0\},\ \{C_2^{(y)} \mid \tfrac{1}{2}\vec{t}_y\},\ \{\sigma_v^{(yz)} \mid \tfrac{1}{2}(\vec{t}_x+\vec{t}_y+\vec{t}_z)\},\\ &\{\sigma_v^{(xy)} \mid \tfrac{1}{2}(\vec{t}_x+\vec{t}_z)\};\\ &\{I \mid 0\},\ \{C_2^{(x)} \mid \tfrac{1}{2}(\vec{t}_x+\vec{t}_y+\vec{t}_z)\},\\ &\{C_2^{(z)} \mid \tfrac{1}{2}(\vec{t}_x+\vec{t}_z)\},\ \{\sigma_v^{(zx)} \mid \tfrac{1}{2}\vec{t}_y\}; \end{aligned} \tag{A1}$$

where E and I are the identity and inversion operators, and $C_2^{(i)}$ and $\sigma_v^{(jk)}$ represent the two-fold rotation about the i axis and the reflection with respect to the jk plane, respectively. The latter factor in each operation represents the nonprimitive translation. Thus, the space group D_{2h}^{16} has three screw axes and three glide planes. The space group C_{2v}^9 (ferroelectric phase) is a subgroup of D_{2h}^{16} and its symmetry operations are the first four operations in (A1). It should be noticed here that the crystal $\vec{c}$ axis of SbSI is taken as parallel to the $\vec{y}$ axis in (A1).

The group D_{2h}^{16} has been studied by Slater[18] by the

TABLE XVII. Compatibility relations between D_{2h}^{16} and C_{2v}^{9}.

D_{2h}^{16}	Γ_1	Γ_2	Γ_3	Γ_4	Γ_5	Γ_6	Γ_7	Γ_8	X_1	X_2	Y_1		Y_2		Z_1	Z_1
C_{2v}^{9}	Γ_1	Γ_3	Γ_3	Γ_1	Γ_2	Γ_4	Γ_4	Γ_2	X_1	X_1	Y_1+Y_4		Y_2+Y_3		Z_1	Z_1
D_{2h}^{16}	R_1		R_2		S_1	S_2	T_1	T_2	U_1	U_2	U_3	U_4	U_5	U_6	U_7	U_8
C_{2v}^{9}	R_1+R_4		R_2+R_3		S_1	S_1	T_1	T_1	U_1	U_2	U_2	U_1	U_3	U_4	U_4	U_3
D_{2h}^{16}	Σ_1	Σ_2	Σ_3	Σ_4	Δ_1	Δ_2	Δ_3	Δ_4	B_1	D_1	F_1	F_2	F_3	F_4	H_1	
C_{2v}^{9}	Σ_1	Σ_2	Σ_2	Σ_1	Δ_1	Δ_2	Δ_3	Δ_4	B_1	D_1	F_1	F_2	F_3	F_4	H_1+H_2	
D_{2h}^{16}	Λ_1	Λ_2	Δ_3	Δ_4												
C_{2v}^{9}	Λ_1	Δ_1	Δ_2	Δ_2												

use of the projection operator defined as

$$f_{jl}^{(p)} = \frac{1}{g} \sum_R \Gamma_p(R)_{jl}^{*} R\Phi , \qquad \text{(A2)}$$

where $\Gamma_p(R)_{jl}$ is the (j,l)th matrix element of the symmetry operation R in the pth irreducible reresentation of the group, and g is the order of the group. Eq. (A2) means that the jth basis function transforming according to the pth irreducible representation can be obtained from any function Φ by this equation. Taking the plane wave as Φ, Slater has obtained the matrix element of all the irreducible representations of the group of $\vec{k}$ of D_{2h}^{16} by the trial-and-error method. The results for the characters are reproduced in Table XIII, where the nonprimitive translational part is omitted from each symmetry operation for simplicity. The same method can be applied for the group C_{2v}^{9}; whose character tables are given in Table XIV. Furthermore, since both groups D_{2h}^{16} and C_{2v}^{9} are the nonsymmorphic space groups, the time-reversal (TR) operation is very important for the groups of $\vec{k}$ on the surface of the Brillouin zone. The degeneracy due to the TR operation is summarized in each table.

The compatibility relations between the symmetry points and lines can be easily obtained from the character tables, and the results for D_{2h}^{16} and C_{2v}^{9} are given in Tables XVI and XVII, respectively. Since the group C_{2v}^{9} is a subgroup of the group D_{2h}^{16}, there is another compatibility relation between these two groups, which is given in Table XVIII.

The simplified one-double-chain model of SbSI described in Sec. IV is characterized by its space group of C_{2h}^{2}. The group C_{2h}^{2} is also a subgroup of D_{2h}^{16} and thus its character tables and compatibility relations can be obtained in the same way as the group C_{2v}^{9}.

In the band calculations at the symmetry points and lines by the pseudopotential method, the basis functions are the symmetrized plane waves, which can be easily constructed by the projection operator (A2) by choosing the appropriate plane wave as the function Φ. Similarly, if the function Φ is the Bloch sum of the atomic wave functions, Eq. (A2) gives the LCAO bases, whose examples are shown in Table IV. It should be remarked here that the LCAO bases can be directly transformed to the bases of the lattice vibrations if the atomic p_i functions $\Phi_{pi}^{(\alpha)}$ are replaced by the atomic displacements $u_i^{(\alpha)}(i=x,y,z)$ of the atomic species α.[7] Then it is seen from Table IV that in the paraelectric phase there are three Γ_4 phonon modes (α = Sb, S, I) in which the four α atoms displace along the $\vec{y}$ axis (or the crystal $\vec{c}$ axis) in the same way. One of them is the acoustic mode and the other two are the optical modes. These two Γ_4 optical phonons may strongly couple with the electrons, because the electrons can move easily in the crystal $\vec{c}$ axis. This strong electron-phonon coupling may give rise to the cooperative instability of the lattice which corresponds to the ferroelectric phase transition.[29] Thus it is reasonably expected that the two Γ_4 optical phonons become soft at the phase transition. Similarly, the two Γ_1 optical phonons are expected to become soft in the ferroelectric phase.

*Work supported in part by the D.G.R.S.T. under the Contract No. 71.7.28.61.

†Chercheur associé au C.N.R.S. during the Academic year 1971-1972, and also Department of Physics, Faculty of Science, University of Tokyo, Tokyo, Japan,

[1]E. Fatuzzo, G. Harbeke. W. J. Merz, R. Nitsche, H. Roetschi, and W. Ruppel, Phys. Rev. **127**, 2036 (1962).

[2]R. Nitsche and W. J. Merz, J. Phys. Chem. Solids **13**, 154 (1960).

[3]T. A. Pikka and V. M. Fridkin, Fiz. Tverd. Tela **10**, 3378 (1968) [Sov. Phys.-Solid State **10**, 2668 (1969)].

[4]R. Blinc, M. Mali, and A. Novak, Solid State Commun. **6**, 327 (1968).

[5]J. Petzelt, Phys. Status Solidi **36**, 321 (1969).

[6]G. Herbeke, E. F. Steigmeier, and R. K. Wehner, Solid State Commun. 8, 1765 (1970).
[7]M. Balkanski, M. K. Teng, S. M. Shapiro, and M. K. Ziolkiewicz, Phys. Status Solidi **44**, 355 (1971).
[8]D. K. Agrawal and C. H. Perry, Phys. Rev. B 4, 1893 (1971).
[9]M. K. Teng, M. Balkanski, and M. Massot, Phys. Rev. B 5, 1031 (1972).
[10]Y. Yamada and H. Chihara, J. Phys. Soc. Jap. **21**, 2085 (1966).
[11]D. V. Chepur, D. M. Bercha, I. D. Turyamitsa, and V. Yu. Slivka, Phys. Status Solidi **30**, 461 (1968).
[12]I. Ya. Nikiforov and A. G. Khasabov, Fiz. Tverd. Tela **13**, 3589 (1971) [Sov. Phys.-Solid State **13**, 3030 (1972)].
[13]G. Harbeke, J. Phys. Chem. Solids **24**, 957 (1963).
[14]V. M. Fridkin, K. Gulyamov, V. A. Lyakhovitskaya, V. N. Nosov, and N. A. Tikhomirova, Fiz. Tverd. Tela **8**, 1907 (1966) [Sov. Phys.-Solid State **8**, 1510 (1966)].
[15]K. Ohi, J. Phys. Soc. Jap. **25**, 1369 (1968).
[16]D. M. Bercha, V. Yu. Slivka, N. N. Syrbu, I. D. Turyanitsa, and D. V. Chepur, Fiz. Tverd. Tela **13**, 276 (1971) [Sov. Phys.-Solid State **13**, 217 (1971)].
[17]Y. Sasaki, Jap. J. Appl. Phys. **3**, 558 (1964).
[18]J. C. Slater, *Quantum Theory of Molecules and Solids* (McGraw-Hill, New York, 1965), Vol. 2, p. 438.
[19]A. Kikuchi, Y. Oka, and E. Sawaguchi, J. Phys. Soc. Jap. **23**, 337 (1967).
[20]E. Dönges, Z. Anorg. Allg. Chem. **263**, 112 (1950).
[21]R. Arndt and A. Niggli, Naturwissenschaften **51**, 158 (1964).
[22]M. L. Cohen and V. Heine, *Solid State Physics*, edited by F. Seitz, D. Turnbull, and H. Ehrenreich (Academic, New York, 1970), Vol. 24, p. 37.
[23]S. H. Wemple, Phys. Rev. B **2**, 2679 (1970).
[24]L. M. Falicov and P. J. Lin, Phys. Rev. **141**, 562 (1966),
[25]K. Nakao, J. Phys. Soc. Jap. **25**, 1343 (1968).
[26]D. Brust, Phys. Rev. 134, A1337 (1964).
[27]C. Y. Fong and M. L. Cohen, Phys. Rev. **185**, 1168 (1969).
[28]H. Kamimura, S. M. Shapiro, and M. Balkanski, Phys. Lett. A 33, 277 (1970).
[29]N. Kristoffel and P. Konsin, Phys. Status Solidi **28**, 731 (1968).
[30]J. D. Zook and T. N. Casselman, Phys. Rev. Lett. **17**, 960 (1966).
[31]Y. W. Tsang and M. L. Cohen, Phys. Rev. B 3, 1254 (1971).